Nano-/microstructure of extruded Spirulina/starch foams in relation to their textural properties

Marta Martinez-Sanz, Emanuel Larsson, Kalep Filli, Camille Loupiac, Ali Assifaoui, Amparo Lopez-Rubio, Patricia Lopez-Sanchez

NANO-/MICROSTRUCTURE OF EXTRUDED SPIRULINA/STARCH FOAMS IN RELATION TO THEIR TEXTURAL PROPERTIES

Marta Martínez-Sanz[a*], Emanuel Larsson[b], Kalep B Filli[b], Camille Loupiac[c,d], Ali Assifaoui[c], Amparo López-Rubio[a] and Patricia Lopez-Sanchez[b]

[a] Food Safety and Preservation Department, IATA-CSIC, Avda. Agustin Escardino 7, 46980 Paterna, Valencia (Spain).

[b] Product Design and Percerption, Agrifood and Bioscience, RISE Research Institutes of Sweden. SE-412 76, Gothenburg (Sweden).

[c] Equipe PCAV, UMR PAM A 02.102, AgroSup Dijon, Univ. Bourgogne Franche-Comté, F-21000 Dijon, France.

[d.] Laboratoire Léon Brillouin, UMR 12, CEA-CNRS, Gif Sur Yvette, France.

*Corresponding author: Tel.: +34 963200022; fax: +34 963636301

E-mail address: mmartinez@iata.csic.es

Abstract

This work reports on an in-depth characterization of the nano- and microstructure of extruded starch foams loaded with the microalga *Spirulina* (1, 5 and 10 wt.%), as well as the implications of *Spirulina* incorporation on the textural properties of the foams. Due to the gelatinization process occurring during extrusion, the crystalline and lamellar structures originally present in the starch granule were disrupted, resulting in very amorphous foams. Moreover, the crystalline structure of the fatty acids present in the raw microalga was lost during processing. The presence of *Spirulina* intracellular components induced the formation of more thermally-stable V-type crystallites through complexation with amylose, hence producing slightly more crystalline foams (X_C~5-9%) than the pure extruded starch (X_C ~3%). This affected the microstructure of the hybrid foams, which showed more densely packed and well-connected porous structures. Microstructural changes had an impact on the texture of the foams, which became harder with greater *Spirulina* loadings. The foams underwent very limited re-crystallization upon storage, which was further reduced by the presence of *Spirulina*. Interestingly, the free fatty acids from *Spirulina* re-crystallized and the resistant starch content in the 10% *Spirulina* foam increased, which could potentially be interesting from a nutritional perspective. These results show the potential of extrusion cooking to produce healthier snack foods and highlight the suitability of advanced characterization tools such as neutron tomography and small angle X-ray scattering to investigate food structure.

Keywords: microalgae; SAXS; WAXS; neutron tomography; gelatinization

1. Introduction

Extrusion cooking is one of the processing methods used in the food industry to produce healthier snack foods, which is increasingly being used to replace conventional technologies such as frying. The process is based on the application of high temperature, pressure and shear stress, resulting in major structural changes (such as starch gelatinization, protein denaturation, formation of amylose-lipid complexes and degradation of bioactive substances) in the raw materials added to the extruder (Camire, Camire, & Krumhar, 1990). After the cooking step, the melt fluid is shaped into the desired form in the die, thus yielding the final product. The properties of the manufactured products can be adjusted by modifying the processing parameters (such as feed moisture, temperature profile, screw speed and feed rate) (Ding, Ainsworth, Plunkett, Tucker, & Marson, 2006; Ding, Ainsworth, Tucker, & Marson, 2005; Hashimoto & Grossmann, 2003) and by selecting suitable raw materials. Cereal flours, rich in starch, are typically the main component in the formulations used to produce extruded snacks, since they present good processability and enable the production of snacks with acceptable physical characteristics, i.e. an adequate expansion coefficient, hardness and density (Guy, 2001; Launay & Lisch, 1983). However, they present low nutritional value due to their relatively limited protein content and deficiency in certain essential amino acids (Bressani, Wilson, Béhar, & Scrimshaw, 1960; Howe, Jansen, & Gilfillan, 1965). In order to improve their nutritional profile, starch-based snack foods have been enriched with several protein-rich ingredients such as legumes and dairy (Anton, Gary Fulcher, & Arntfield, 2009; Onwulata, Konstance, Smith, & Holsinger, 2001; Rampersad, Badrie, & Comissiong, 2003; Veronica, Olusola, & Adebowale, 2006). However, the incorporation of these additional ingredients into the extrusion formulations does not only have an impact from the nutritional perspective, but also has technological implications, since the processing parameters need to be adjusted and the structural, textural and sensory

properties of the extruded snacks may be affected (Lazou & Krokida, 2010; Pastor-Cavada, et al., 2011).

Besides demanding products with added nutritional value and health benefits, consumers are increasingly searching for more natural ingredients, such as algae-based products. In this context, microalgae are gaining a great interest in the food industry for their use as nutritional supplements and food additives (Chacón-Lee & González-Mariño, 2010; Vigani, et al., 2015). Some microalgae species have been used in human nutrition for many centuries and the interest lays in their high protein content, lipid profile, with relatively high amounts of ω3 and ω6 fatty acids, and the presence of bioactive compounds such as carotenoids, phycobilins, polysaccharides, vitamins, and sterols (Chacón-Lee, et al., 2010; Spolaore, Joannis-Cassan, Duran, & Isambert, 2006). In particular, *Spirulina*, filamentous blue-green microalgae or cyanobacteria, are one of the most widely used species in the healthy-food market due to their large content in proteins, γ-linolenic acid and other compounds such as vitamins (mainly B vitamins), minerals, pigments (phycocyanin, β-carotene and xanthophyll), γ-tocopherol and phenolic compounds, which confer these microalgae high antioxidant activities (Khan, Bhadouria, & Bisen, 2005; Miranda, Cintra, Barros, & Mancini-Filho, 1998). Since these microalgae have received the GRAS (Generally Recognized As Safe) certification, they have already been incorporated into different types of food products, such as shakes for elderly (Santos, Freitas, Moreira, Zanfonato, & Costa, 2016), pasta (De Marco, Steffolani, Martínez, & León, 2014; Fradique, et al., 2010; Özyurt, et al., 2015) and extruded snacks (Joshi, Bera, & Panesar, 2014; Bárbara Franco Lucas, de Morais, Santos, & Costa, 2018; Barbara Franco Lucas, Morais, Santos, & Costa, 2017; Morsy, Sharoba, & Hem, 2014). Although most of the existing literature has focused on the nutritional aspects, the incorporation of *Spirulina* may have an

impact on the structural changes undergone by food during processing. This may be especially important in the case of starchy foods, whose processing is based on the occurrence of a phenomenon known as gelatinization. Native starch granules display a hierarchical structure consisting of alternating amorphous and semi-crystalline growth rings of 120–400 nm thickness. At the same time, the semi-crystalline rings are formed by a lamellar structure of alternating crystalline and amorphous regions with a repeat distance of 9–10 nm (Blazek & Gilbert, 2011). When processed at high temperature and moisture conditions, starch is known to undergo a gelatinization process in which its hierarchical structure is disrupted. The gelatinization process is initiated by the access of water towards the interior of starch granules, which swell and absorb water, followed by the disruption of the crystalline and lamellar structure and the leakage of amylose from the starch granules to form a continuous gel. In fact, it has been recently demonstrated that *Spirulina* microalgae interfere with the gelatinization process of starch and as a result, lipid-amylose complexes can be formed, promoting the crystallisation of V-type structures (Martínez-Sanz, Fabra, G. Gómez-Mascaraque, & López-Rubio, 2018). Thus, the incorporation of *Spirulina* into starch-based snack foods is not only expected to impact the nutritional value, but also to affect the structural properties of the obtained products. In this study we have performed a detailed investigation of the structural effects of the addition of *Spirulina* into corn starch foams produced by means of extrusion cooking. For the first time a combination of advanced characterisation techniques (ranging from the nanometre to micrometre length scale), such as X-ray scattering (SAXS/WAXS) and neutron tomography, together with scanning electron microscopy (SEM), were used to understand the structural changes occurring in extruded starch foams as result of the addition of *Spirulina* microalgae. Some of the main advantages of using scattering and tomography techniques are related to their non-destructive character and their ability able to provide structural information on native

samples, since they minimise experimental artefacts derived from sample treatment. Furthermore, the use of neutrons is particularly interesting for the analysis of food systems by means tomography due to the higher contrast of neutrons with hydrogens (abundant in food components), as compared with X-rays. These results are highly relevant in the development of new food products, since structural changes are expected to affect the sensory properties and digestibility of the produced snacks.

2. Materials and methods

2.1 Materials

Commercial corn starch flour (19% amylose) was purchased locally (Sweden). *Spirulina platensis*, in the form of dry powder, was kindly donated by Dr. Acién from the University of Almeria (Spain). The composition of the raw *Spirulina* in terms of total carbohydrate, protein, ash, lipids and polyphenols was determined using standard methods. The total carbohydrate content was determined after sulphuric acid hydrolysis, following the method described in previous work (Martínez-Sanz, et al., 2019). The protein content was determined by the Kjeldahl method, using a factor of 6.25 to convert the nitrogen to protein content (Boussiba & Richmond, 1979). The ash content was determined by the standard method TAPPI T211 om-07. Lipids were estimated by performing a Soxhlet extraction of ca. 1g of dry *Spirulina* with 800 ml of toluene:ethanol 2:1 (v/v) for 24 h. The total phenolic content was estimated by the Folin-Ciocalteau colorimetric assay (Singleton, Orthofer, & Lamuela-Raventós, 1999). The gross chemical composition of the microalgal biomass was determined as: 40.6% ash, 26.7% protein, 15.1% lipid; 8.0% carbohydrate and 0.9% polyphenols.

2.2 Preparation of starch and starch-*Spirulina* foams

Pure starch and hybrid foams with three different loadings of *Spirulina* (1, 5 and 10 wt.% dry weight) were prepared by extrusion cooking. The samples were processed with 30 wt.% moisture content to facilitate starch gelatinization during processing and let to equilibrate for 24 hours before extrusion. A single-screw extruder (Brabender Duisburg DCE-330, Germany) equipped with a variable speed D-C drive unit was used. The extruder barrel had a 25 mm diameter with length to diameter ratio (L: D) of 20:1. The screw was a 2:1 compression ratio with a linearly tapered rod and 20 equidistantly positioned flights. A round circular die with a 2 mm diameter and a length of 90 mm was used. Extrusion temperature was kept constant at 120 °C, 150 °C, 150 °C and 140 °C for zones 1, 2, 3 and 4 respectively. A screw speed of 150 rpm was used for all extrusion processes. The extrudates were collected when the operation conditions were at constant steady state. Each formulation was processed twice. The obtained samples were stored in an equilibrated relative humidity cabinet at 30% RH and 14 ºC for two-three days (T0) and one month (TF) prior to their characterization. Expansion index was calculated as the ratio of the diameter of the extruded sample to the diameter of the die.

2.3 Attenuated total reflectance (ATR) FT-IR analysis

Small pieces from the produced foams were grounded into powder and the obtained materials were analysed by FT-IR in attenuated total reflectance (ATR) mode using a Thermo Nicolet Nexus (GMI, USA) equipment. The spectra were taken at 4 cm^{-1} resolution in a wavelength range between 400-4000 cm^{-1} and averaging a minimum of 32 scans.

2.4 Determination of resistant starch content

Resistant starch content was measured using the Megazyme Resistant Starch Assay Kit (Megazyme International, Wicklow, Ireland), based on the AACC method 32-40.01 (AACC,

2009). Extruded samples were grounded to a fine powder in a blender. The samples (100 mg) were incubated with 4 mL mixture of pancreatic α-amylase and amyloglucosidase for 16 h (at 37 °C, 200 strokes/min) in a shaking water bath (Julabo, Seelbach, Germany) to hydrolyze digestible starch to glucose. The reaction was terminated with 4 mL of 99 % ethanol and the indigested resistant starch fraction was obtained after centrifugation (1500 ×g, 10 min). The residue was washed twice with 50 % ethanol and solubilized with 2 mL of KOH solution 2 M in an ice bath. The solution was neutralized after 20 min with 8 mL sodium acetate buffer (1.2 M, pH 3.8), and incubated with amyloglucosidase (0.1 mL, 3300 U/mL) at 50 °C for 30 min. Aliquots (0.1 mL) of the diluent were taken and mixed with 3 mL of glucose oxidase/peroxidase reagent (GOPOD) and the mixture was incubated at 50°C for 20 min. Absorbance at 510 nm was measured using a spectrophotometer (Ultrospec, Biochrom, Cambridge, Germany). The samples were measured in duplicates and two different batches of extruded samples were assessed. Resistant starch was calculated as g per 100 g of dry sample.

2.5 Scanning electron microscopy (SEM)

SEM measurements were conducted on a Hitachi microscope (Hitachi S-4800) at an accelerating voltage of 10 kV and a working distance of 8-16 mm. The pure and composite starch films were cryo-fractured after immersion in liquid nitrogen to observe the cross-sections. The samples were then sputtered with a gold–palladium mixture under vacuum during 3 minutes before their morphology was examined.

2.6 Simultaneous small and wide angle X-ray scattering (SAXS/WAXS) experiments

Combined small and wide angle X-ray scattering (SAXS and WAXS, respectively) experiments were carried out in the Non Crystalline Diffraction beamline, BL-11, at the

ALBA synchrotron light source ("ALBA synchrotron"). The obtained foams were characterized shortly after being processed (t_0) and after prolonged storage at 30% RH (t_f), both in their native dry state and after being hydrated in excess water for at least 24 h. The energy of the incident photons was 12.4 KeV (an equivalent wavelength, λ, of 1 Å). The SAXS diffraction patterns were collected by means of a single-photon counting detector, Pilatus 1 M, with an active area of 168.7×179.4mm^2, an effective pixel size of 172×172 μm^2 and a dynamic range of 20 bits. The sample-to-detector distance was set to 7740 mm, resulting in a q range with a maximum value of q=0.189 Å^{-1}. The WAXS diffraction patterns were collected by means of a 3 CCD detectors, Rayonix LX255-HS, with an active area of 85×255mm^2, an effective pixel size of 44×44 μm^2 and a dynamic range of 16 bits. In this case, the sample-to-detector distance was set to 144.3 mm, corresponding to a maximum q value of 8.023 Å^{-1}. This detector was tilted with a pitch of 29.38°. The exposure time, common to both detectors, was 2 s. This time was optimized in preliminary measurements, in order to maximize the signal to noise ratio while avoiding detector saturation.

2.7 SAXS/WAXS data fitting

SAXS data were fitted using the Igor NIST analysis macro suite (Kline, 2006) and applying a mathematical function consisting of a power-law term plus one Gaussian-Lorentzian peak, similar to that previously reported for several starch samples (A. Lopez-Rubio, et al., 2007; Salman, et al., 2009):

$$I(q) = A \cdot q^{-m} + \left[R \cdot \left[I_{max} \cdot \left(1 + \left(\frac{2\cdot(q-q_{max})}{\Delta q}\right)^2\right)^{-1}\right]\right] + \left[(1-R) \cdot \left[I_{max} \cdot exp\left[-\frac{1}{2} \cdot \left(\frac{q-q_{max}}{\Delta q}\right)^2\right]\right]\right] + bkg \quad (1)$$

The first term in equation (1) corresponds to the power-law function (where A is a prefactor and m is the power-law exponent) to account for the underlying diffuse scattering, the second and third terms correspond to the Lorentzian and Gaussian functions used to describe the starch lamellar peak (where q_{max} is the peak position, I_{max} is the intensity of the peak, Δq is the full width at half maximum and R is the Lorentzian to Gaussian ratio of the peak shape) and the fourth term accounts for the incoherent background signal.

WAXS peak fitting was performed in Igor, following the procedure described in a previous work (Amparo Lopez-Rubio, Flanagan, Gilbert, & Gidley, 2008). The obtained values from the fitting coefficients are those that minimize the value of Chi-squared, which is defined as:

$$\chi^2 = \sum \left(\frac{y - y_i}{\sigma_i}\right)^2 \quad (2)$$

where y is a fitted value for a given point, y_i is the measured data value for the point and σ_i is an estimate of the standard deviation for y_i. The curve fitting operation is carried out iteratively and for each iteration, the fitting coefficients are refined to minimize χ^2. The crystallinity index X_C was determined from the obtained fitting results by applying the following equation:

$$X_C(\%) = \frac{\sum A_{Crystal}}{A_{Total}} \times 100 \quad (3)$$

where A_{Total} is the sum of the areas under all the diffraction peaks and $\Sigma A_{Crystal}$ is the sum of the areas corresponding to the crystalline peaks.

2.8 Neutron tomography

2.8.1 Data acquisition

Neutron tomography experiments were performed at the cold neutron imaging station, IMAGINE (Ott, Loupiac, Désert, Hélary, & Lavie, 2015) at the ORPHEE reactor of the French national neutron facility, the *Léon Brillouin Laboratory* (Saclay, France). The 4 types of foams produced by extrusion were scanned: pure starch (n=2), 1% *Spirulina* (n=3), 5% *Spirulina* (n=3) and 10% *Spirulina* (n=3), where n equals the number of scanned samples. The scanning parameters were the following: exposure time, 60s and number of projections, 180; number of dark and flat-field projections, 10; sample-to-detector distance, 50 mm; field of view (FOV), 47mm × 40mm; effective isotropic pixel size, 18.5 µm. The characteristics of the utilized detector setup were the following; a Neo sCMOS (ANDOR) camera equipped with a sCMOS sensor (effective number of pixels, 2560 x 2160 pixels^2; physical pixel size: 6.5 x 6.5 µm^2) coupled to a 50µm thick gadolinium scintillator (RC Tritec, 2014), followed by optimal light magnification using a 35 mm objective (Canon EF 35 mm f/2.0 IS USM). Furthermore, the camera was cooled down to -30°C, to reduce noise. Pieces of few centimeters of the extruded samples (T0) were placed in an aluminum film inside a cylindrical aluminum cell placed in front of the scintillator on the rotating table.

2.8.2 Image pre-processing and 3D reconstruction

An in house-developed macro from the IMAGINE imaging station and implemented in ImageJ (Rueden, et al., 2017) was used to normalize the projection images, remove noise and correct the tilt-angle. Hereinafter, the SYRMEP Tomo Project (STP) (Brun, et al., 2017) was used to reconstruct a 3D-map of the linear attenuation coefficient (LAC) [cm^{-1}] of the neutrons for the scanned samples. The LAC was reconstructed on 32-bit grey-level scale.

2.8.3 Image post processing

The reconstructed slices contained two well-separated peaks, associated to air and starch/*Spirulina*. Standard grey-level thresholding was shown to be unable to accurately segment the foams, due to the large variance in grey-scale values between the thinner and thicker cell wall structures, as shown in Figure S1A. Therefore, an automated (supervised) pixel-level classification method (based on intensity, edge and texture with sigma = 0.7) implemented in the Ilastik software framework (Sommer, Straehle, Koethe, & Hamprecht, 2011) was applied. One slice from each type of sample group was used for combined training, wherein after the automated segmentation method was applied to all respective slices of the given data sets, as shown in Figure S1B.

In extrusion, both the material composition and the utilized processing parameters determine the pore size and cell wall thickness. Consequently, samples with a very thin outer cell wall thickness tend to rupture easily, as shown in (Bárbara Franco Lucas, et al., 2018). The open path between the air outside and inside the sample respectively hampers more advanced image analysis, especially so called skeletonization, followed by the calculation of the Connectivity Density (Conn.D). Therefore, an image processing protocol implemented in ImageJ, which successfully closes the open path at broken cell walls, was developed and applied to all of the hereby addressed data sets, as shown in Figure S1.

2.8.4 Quantitative 3D image analysis

Quantitative 3D image analysis was performed using the Pore3D software library (Brun, et al., 2010) on Representative Volume of Interest (RVI) of the respective data sets, following an RVI-test, as further described in the Supplementary Material section 'Representative Volume of Interest (RVI) test'. The following image parameters were quantified: 1) Volume percentage (Vol. Perc.) of the air part, also referred to as 'porosity', 2) Specific Surface Area,

computed as the quotient between the surface area of the object divided with the total volume of the VOI as further described by (Parfitt, et al., 1987), 3) Structure Thickness (St.Th.) of the extruded foams, hereinafter referred to as 'cell wall thickness' and 4) Conn.D, as well as 5) pore and 6) throat sizes, based on skeletonization, as further described in (Furlan, et al., 2018), hereinafter referred to as Method 1. For objective comparison, the pore size was also estimated on the individually separated macro pores, by applying a 'Distance Transform Watershed 3D' algorithm in the MorphLibJ package (Legland, Arganda-Carreras, & Andrey, 2016) in ImageJ, using the following parameters: Borgefors(3,4,5) and 'normalization dynamic': 6.0, followed by quantification using Pore3D, hereinafter referred to as Method 2. However, only Method 1 is capable of estimating both the pore and the throat size.

2.8.5 3D Visualization

The 3D volume renderings were performed using the Drishti package for visualization of volumetric datasets (Limaye, 2012) and using 'Volume viewer' in ImageJ (Rueden, et al., 2017) for visualization of the 'local thickness' (Hildebrand & Rüegsegger, 1997), as well as the individually separated macro pores, as separated by 'Wathershedding'.

2.9 Uniaxial Compression testing

Uniaxial compression tests were performed on an Instron material testing device (model 5542, Instron, Norwood, MA, USA). Extruded samples were carefully cut to cylindrical shapes with a height of ca. 1 cm with the help of a sharp scalpel and placed between flat metal surfaces covered with emery paper to avoid slippage. A 3 cm cylindrical probe was used to compress the samples until fracture, using a 500 N load cell (load values during compression were in the range of 125-200 N) at a crosshead speed of 1 mm/s. At least 5

replicates of each type of extruded sample were measured. Force (N) and distance (mm) were converted to true stress (σ_T) and true strain (ε_T) using equations 1 and 2 by the instrument software Blue Hill.

$$\sigma_T = \frac{F(t)(h_0 - \Delta h(t))}{\pi r_0^2 h_0} \quad (4)$$

$$\varepsilon_T = \ln\left(\frac{h_0}{h_0 - \Delta h(t)}\right) \quad (5)$$

Where h_0 is the initial height of the sample, $\Delta h(t)$ is the change in height during compression and r_0 is the initial radius of the sample. The compression modulus was obtained as the slope of the initial linear zone of the true stress vs. true strain plots. Mean values of the critical stress and the compression modulus were compared by Tukey and Fisher tests with a confidence interval of 95% using Excel Stats software.

3. Results and Discussion

3.1 Nanostructure of the as-processed foams

In this work, different contents of *Spirulina* (1, 5 and 10 wt.%) were incorporated into corn starch formulations to produce foams by means of extrusion cooking. To investigate the effects of the added microalgae on the structure of the foams, the samples were characterized by wide angle and small angle X-ray scattering (WAXS and SAXS). These techniques are very powerful tools to extract information on the lamellar and crystalline arrangement of starch, as widely reported in the literature (Blazek, et al., 2011; P. Jenkins, et al., 1994).

The WAXS patterns of the raw materials and the as-processed foams (T0) are shown in Figure 1A. As observed the raw corn starch presented WAXS patterns typical from the A-type crystalline allomorph, characterized by the main diffraction peaks located at 2θ = 15.1º, 17.0º, 18.1º and 23.1º. On the other hand, the raw *Spirulina* presented several sharp peaks,

of which the most intense ones were located at 2θ values of ca. 20.6º, 29.1º, 29.6º, 30.9º, 31.7º, 38.0º, 41.8º and 47.1º the most intense ones. The appearance of these peaks has been previously associated to the presence of crystallized fatty acids in this microalga (Martínez-Sanz, et al., 2018), although they have not been assigned to any particular crystalline allomorph yet. In fact, the crystallinity of the raw *Spirulina* is very close to the total amount of lipids determined in the sample (ca. 15%), thus supporting the hypothesis of crystallized fatty acids present in the native microalga. After the extrusion cooking process, a very amorphous structure, showing a WAXS pattern resembling the characteristic pattern of the V-type crystalline allomorph, was observed for the pure starch foam. Interestingly, the position and relative intensity of the scattering peaks did not correspond to any of the reported pure V-type crystalline structures. This is in agreement with a previous study which demonstrated that corn starch samples shortly after being processed by extrusion presented a non-stable structure consisting of a mixture of different crystalline allomorphs (Benito-González, López-Rubio, & Martínez-Sanz, 2019). The samples containing *Spirulina* showed scattering patterns similar to those reported for V-type starches and displayed greater crystallinity values than the pure starch foam (cf. Table 1). The application of heat/moisture treatments is known to induce the formation of V-type crystalline structures in corn starch due to the complexation of the fatty acids and phospholipids naturally present in the raw cereal with the amylose chains from starch (Kugimiya, Donovan, & Wong, 1980; Zobel, 1988). Our results indicate that the formation of V-type crystallinity was clearly favoured by the presence of *Spirulina*. The weak cell walls from *Spirulina* have been seen to break down very easily, even with only mild stirring (Fabra, et al., 2017; Martínez-Sanz, et al., 2018), thereby enabling the release of the components contained within the cells, such as lipids and proteins. Furthermore, a previous study showed that the formation of V-type crystallites as the result of lipid-amylose complexation takes place when subjecting corn starch to a high-

362 humidity thermal treatment in the presence of *Spirulina* (Martínez-Sanz, et al., 2018). Thus,
363 it can be assumed that the shearing effect during the extrusion cooking process promoted
364 cell wall disruption and facilitated the release of intracellular components which were able
365 to form complexes with amylose. Moreover, the WAXS results suggest that the formed V-
366 type complexes were more thermally stable than the original A-type crystallites present in
367 the raw corn starch, hence producing slightly more crystalline samples after the extrusion
368 cooking process. This is in agreement with previous work which reported that a small
369 fraction of these V-type crystallites was resistant at 110 ºC (Martínez-Sanz, et al., 2018).
370 Accordingly, the WAXS results suggest that, in parallel with the gelatinization process, the
371 presence of *Spirulina* cell wall components favoured the formation of V-type complexes,
372 which were more thermally stable than the original A-type crystallites present in the raw
373 corn starch. This resulted in the production of slightly more crystalline samples after the
374 extrusion cooking process. It should be noted that none of the peaks detected in the hybrid
375 foams corresponded to those assigned to the raw microalgae, suggesting that the fatty acid
376 crystals were melted upon processing.
377
378 While WAXS is able to provide information on the crystalline structure of starch, SAXS is
379 mostly used to understand the lamellar arrangement. The SAXS patterns from the raw
380 materials and the obtained foams (T0) are shown in Figure 1B. As observed, only the native
381 starch presented a weak and broad lamellar peak centred at ca. 0.071 $Å^{-1}$ in the native dry
382 state, which corresponds to a lamellar repeat distance of ca. 8.8 nm. The identification of the
383 starch lamellar peaks is typically much more evident in hydrated samples. This may be due
384 to the plasticization of amylopectin branch points, increasing the mobility of the amylopectin
385 double helices, which are then able to align in layers (i.e. lamellae), or simply to increased
386 contrast between the amorphous and the semicrystalline lamellae as a result of the easier

387 access of water towards the amorphous part of the granules. On the contrary, in the dry state
388 the amylopectin branch points become less flexible and as a result, their arrangement into
389 lamellae is more limited, although the correlations within the double helices persist (giving
390 rise to the WAXS peaks). Accordingly, the lamellar peak detected in the raw starch became
391 more intense and sharp in the hydrated state and its position shifted towards ca. 0.063 $Å^{-1}$
392 (cf. Figure 1C), corresponding to a lamellar repeat distance of ca. 9.9 nm, in agreement with
393 the lamellar distances previously reported for other corn starches (P. J. Jenkins, Cameron, &
394 Donald, 1993; Kuang, et al., 2017; Martínez-Sanz, et al., 2018). This peak was absent in the
395 patterns from the foams, pointing out towards a disruption of the lamellar structure during
396 the extrusion cooking process, in line with the WAXS results and in agreement with previous
397 works (Benito-González, Martínez-Sanz, & Lopez-Rubio, 2018). This was further
398 confirmed by the change in the power-law exponent from the low q region (0.003-0.005 $Å^{-1}$),
399 which decreased from ca. 4 for the raw starch (corresponding to the Porod's ideal two-
400 phase system and typically reported for native starches (Chanvrier, et al., 2007; Lopez-
401 Rubio, Htoon, & Gilbert, 2007)) to 2.3-2.7 for the foams (corresponding to mass fractal
402 structures). Power-law exponents close to 2 have been reported for gelatinized starches
403 where the lamellar order was completely lost (Lopez-Rubio, et al., 2007), while slightly
404 higher exponents, similar to the values here reported, have been estimated for melt-
405 compounded cellulose-starch samples (Benito-González, et al., 2018). Extrusion of starch
406 samples in excess water has been reported to completely destroy the lamellar structure
407 (Waigh, Gidley, Komanshek & Donald, 2000), whereas a weak 9-10 nm lamellar peak has
408 been seen to remain when the extrusion process was carried out at relatively low water
409 contents (Chanvrier, Uthayakumaran, Appelqvist, Gidley, Gilbert & López-Rubio, 2007).
410 Our results support the fact that the lamellar structure of starch was extensively disrupted

with the addition of 30 wt.% moisture and the conditions used for the extrusion cooking process, both for the pure starch and the blends with the added *Spirulina*.

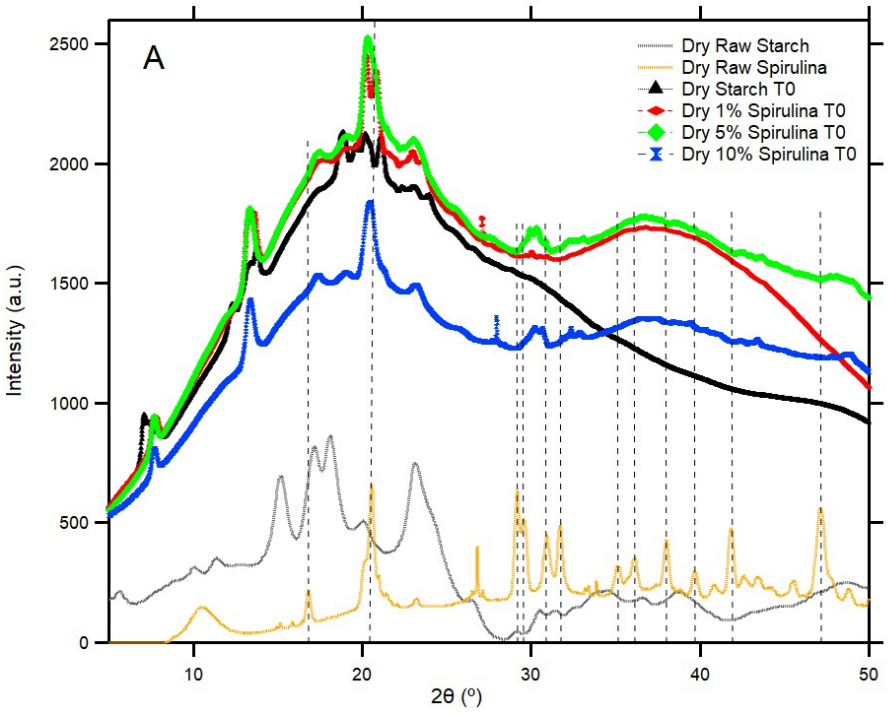

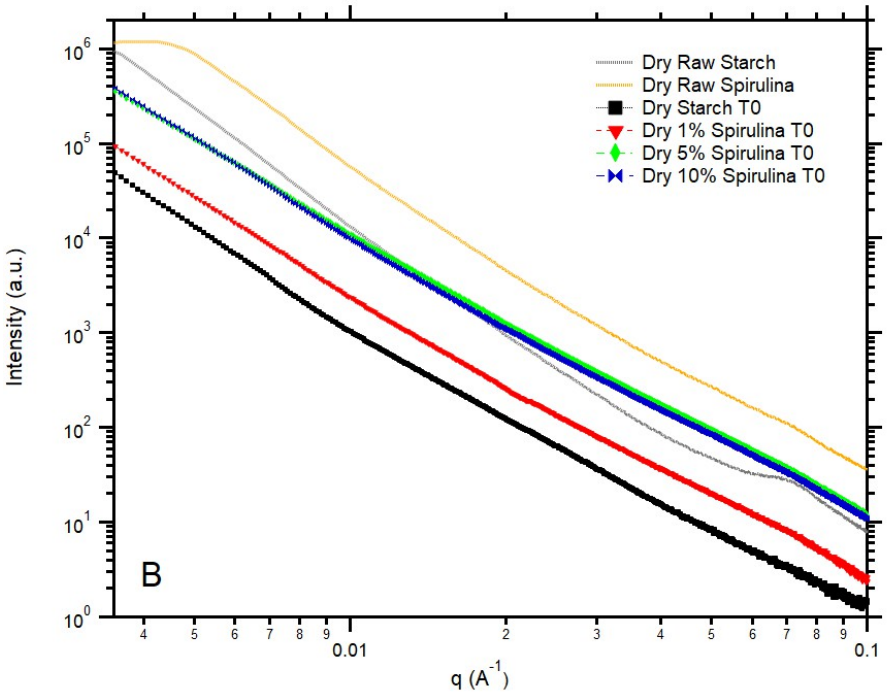

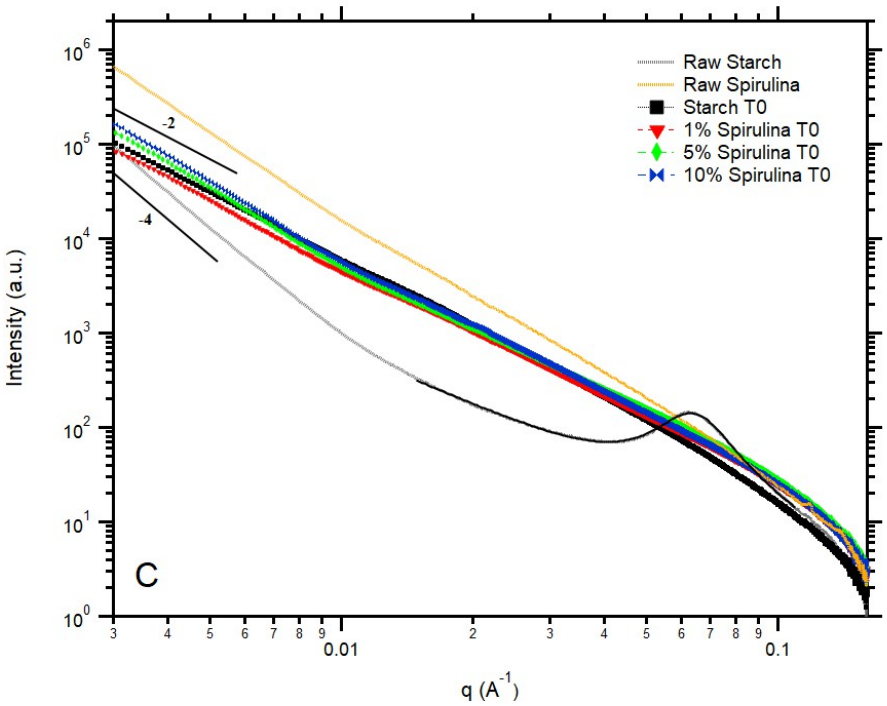

Figure 1. (A) WAXS patterns from the raw starch and *Spirulina* and from the as-processed foams (T0). Curves form raw starch and *Spirulina* have been offset for clarity. (B) SAXS patterns of the raw starch and *Spirulina* and the foams after being processed (T0) in their native dry state and (C) SAXS patterns from the fully hydrated samples. Dotted lines correspond to the experimental data, whereas solid lines correspond to the fitting curves.

Table 1. Power-law exponents, lamellar peak parameters and crystallinity (X_C) for the raw materials and the foams after being processed (T0). The lamellar peak parameters were obtained by fitting the experimental SAXS data of the hydrated samples to the sum function of a power-law plus a Gaussian-Lorentzian peak and crystallinity was obtained from the peak fitting of the WAXS patterns from the dry samples. Standard deviation values on the last digit are shown in parentheses for the fitting parameters.

	Power-law exponent	Lamellar peak position ($Å^{-1}$)	Width of the lamellar peak ($Å^{-1}$)	Lamellar repeat distance (Å)	X_C (%)

Raw *Spirulina*	3.24 (1)	---	---	---	14.98
Raw Starch	2.009 (3)	0.06335 (1)	0.02543 (5)	9.92	42.71
Starch	2.49 (1)	---	---	---	3.22
1% *Spirulina*	2.34 (5)	---	---	---	4.59
5% *Spirulina*	2.52 (1)	---	---	---	6.62
10% *Spirulina*	2.73 (1)	---	---	---	8.72

429

430 **3.2 Microstructure and mechanical properties of the as-processed foams**

431

To understand the effects of *Spirulina* addition at a larger size range, the microstructure of the obtained foams was also investigated by SEM and neutron tomography. Representative SEM images, together with pictures showing the visual appearance of the foams, are shown in Figure 2. As observed, the addition of *Spirulina* produced foams with a greenish coloration, which was more evident for loadings higher than 5 wt.%. Furthermore, as evidenced by the SEM images, more densely packed structures were present in the foams containing higher *Spirulina* loadings. Such effect that was also observed macroscopically.

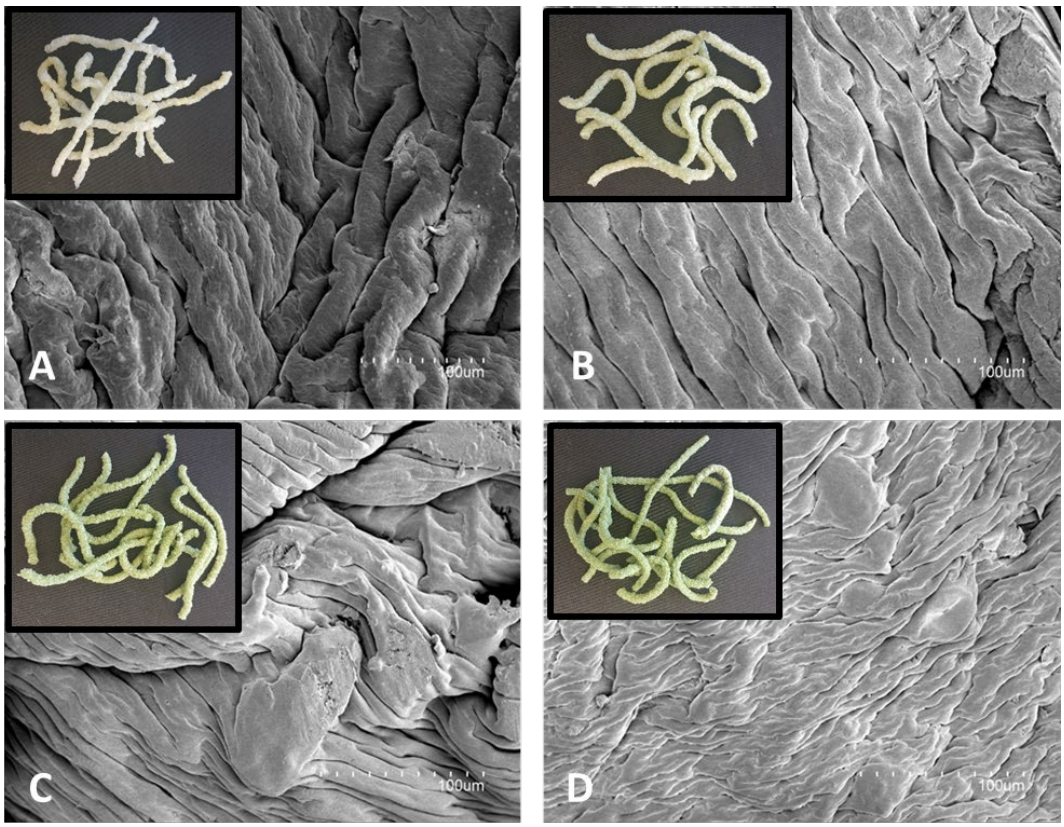

Figure 2. SEM micrographs from the as-processed foams (T0): (A) Pure starch, (B) 1% *Spirulina*, (C) 5% *Spirulina* and (D) 10% *Spirulina*. Image inserts show the visual appearance of the foams.

An in-depth 3D characterization of the microstructure from the different foams was carried out by means of neutron tomography. The porous structure of the extruded foams could be clearly resolved and visualized by this technique, as shown in Figure 3 and Figure 4. The visual results were also supported with quantitative image analysis and the obtained parameters are summarized in Table 2. As observed, loadings higher than 5 wt.% *Spirulina* led to a reduction in the porosity. The specific surface area and connectivity density (Conn.D) increased with increasing concentrations of *Spirulina*, indicating that more well-connected foams were formed. In addition, the cell wall thickness decreased with the addition of *Spirulina*, although there was no clear trend with the microalga concentration (cf. Table 2 and Figure 4). However, no significant differences in pore size or throat size could be measured, due to the large heterogeneity of the samples, which led to large standard deviations. These data have thus been supported by pore and throat size probability distributions, calculated with method 1 and 2, as described in the Supplementary Material section (Figures S4, S5 and S6), indicating that the pore size (mean and standard deviation) decreased with increasing concentration of *Spirulina*.

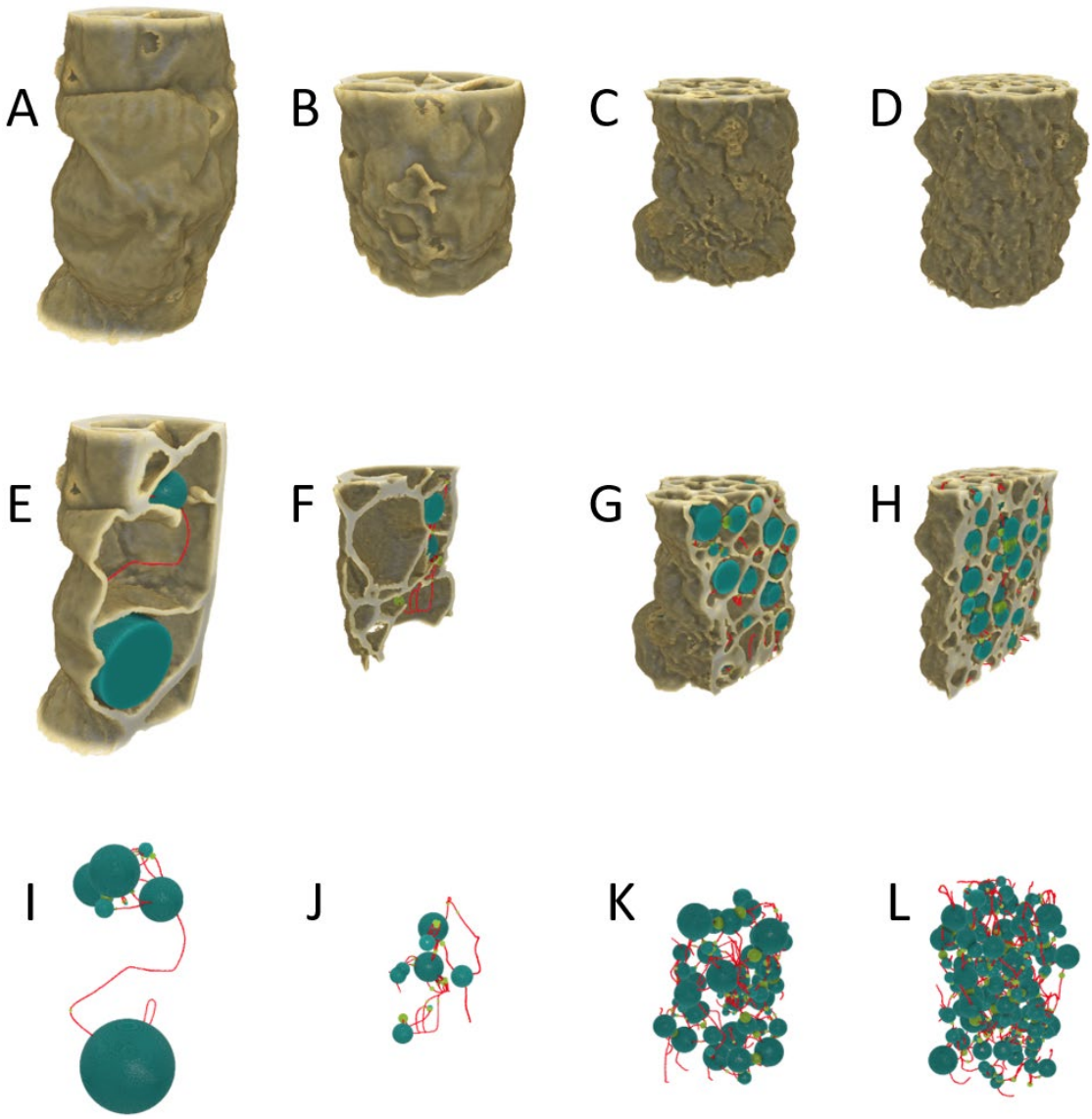

Figure 3. Visualization of the microstructure of the as-processed foams (T0) determined by neutron tomography. (A-D) show volume renderings of the extruded foams (in light brown), (E-H) with applied virtual cut planes. (E-H and I-L) show the longest connected image skeleton (in red) throughout the pore space, with maximal inscribed blobs in the porous part at the nodes (dark green) and at the throats (light green) along the longest skeleton, as described by 'Method 1'. The height of the samples were 11.2 mm and 7.1 mm for the pure starch and the hybrid starch-*Spirulina* samples, respectively. (A, E, I) Pure starch, (B, F, J) 1% *Spirulina*, (C, G, K) 5% *Spirulina* and (D, H, L) 10% *Spirulina*.

Table 2. Extracted image descriptors obtained by applying quantitative 3D image analysis on selected volumes of interests (VOIs), with a representative VOI height of 11.2 mm and 7.1 mm for the pure starch and the hybrid starch-*Spirulina* samples, respectively. See Figures S2 and S3 for details of how the representative volume of interest was selected.

	Porosity (%)	Specific Surface Area (mm^{-1})	Cell wall thickness (µm)	Conn.D (mm^{-3})	Pore Size (µm) Method 1 (Method 2)	Throat Size (µm) Method 1
Starch	67.6 ± 3.1	1.7 ± 0.1	234.0 ± 18.4	0.06 ± 0.00	1109.0 ± 1068.9 (1210.9 ± 922.1)	161.2 ± 114.9
1% *Spirulina*	64.8 ± 1.2	2.5 ± 0.1	199.1 ± 0.2	0.07 ± 0.00	707.7 ± 527.4 (859.9 ± 600.6)	178.0 ± 133.2
5% *Spirulina*	57.2 ± 2.4	3.8 ± 0.1	165.1 ± 1.7	0.34 ± 0.05	652.8 ± 279.1 (671.3 ± 247.9)	152.9 ± 91.9
10% *Spirulina*	50.3 ± 5.0	4.2 ± 0.2	180.1 ± 25.2	0.79 ± 0.09	528.5 ± 198.4 (574.4 ± 196.3)	159.0 ± 92.5

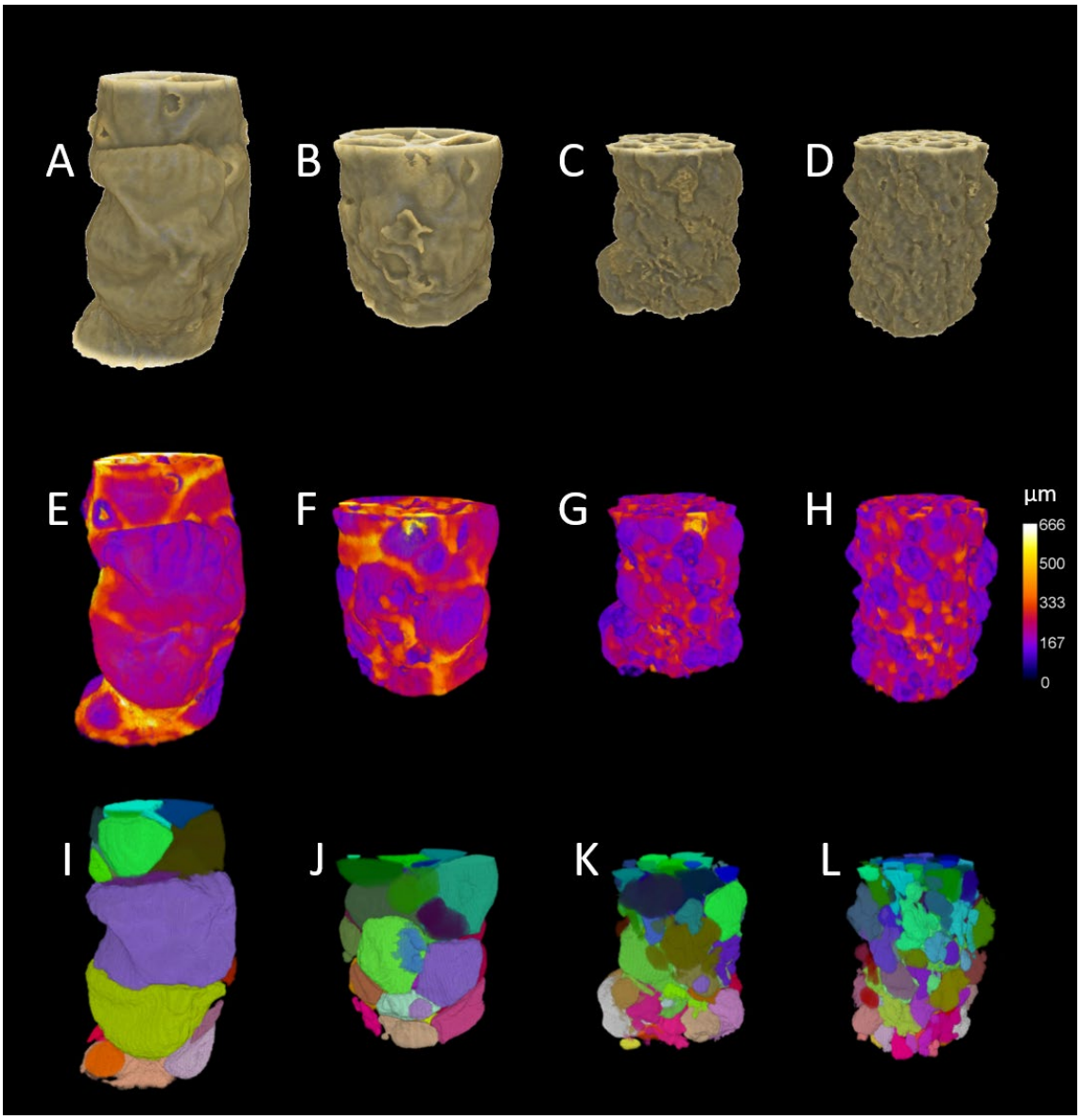

Figure 4. (A-D) Volume renderings of the as-processed foams (T0) (in light brown), as determined by neutron tomography. (E-H) Visualization of the cell wall thickness, which is colour coded, and given in µm. (I-L) Visualization of the individual pores, following 3D water shedding and colour labelling, as described by 'Method 2'. The height of the samples were 11.2 mm and 7.1 mm for the starch and hybrid starch-*Spirulina* foams, respectively. (A, E, I) Pure starch, (B, F, J) 1% *Spirulina*, (C, G, K) 5% *Spirulina* and (D, H, L) 10% *Spirulina*.

The structural changes undergone by starch during the extrusion cooking process were expected to have a strong impact on the mechanical properties of the obtained foams, which in turn are directly linked to their texture. Food texture is a very important attribute from the perspective of consumers' acceptance and thus, it is crucial for the application of these foams as food snacks. The expansion index of the extrudates is directly related to the microstructure of extrudates, and has been shown to be a determining factor for the crunchiness (Joshi, et al., 2014). The expansion index was calculated as described in the materials and methods section and was reduced from 3.1 ± 0.2 for the corn starch to 2.8 ± 0.1, 2.3 ± 0.1 and 2.2 ± 0.1 for the hybrid samples containing 1%, 5% and 10 % *Spirulina,* respectively. These results are in agreeement with previous works which showed no effect on the expansion index of rice and corn flour mixtures (2:1) with the addition of 0.4-2.6 wt.% *Spirulina* (reporting values which ranged from 2.5 to 4.5 depending on the extrussion conditions) (Bárbara Franco Lucas, et al., 2018; Barbara Franco Lucas, et al., 2017; Morsy, et al., 2014), while higher *Spirulina* loadings (6-8%) have been shown to reduce the expansion index (Tańska, Konopka, & Ruszkowska, 2017). As suggested by the WAXS results, the *Spirulina* cell wall components were able to form complexes with amylose during the extrusion cooking process, leading to the formation of more thermally-stable V-type crystallites and, therefore, producing slightly more crystalline foams with reduced elasticity and thus, limited ability to expand. The reduced expansion index of the 5% and 10% *Spirulina* hybrid foams can be directly linked to their more densely packed structures, as observed by SEM and neutron tomography.

Compression experiments were also carried out to determine the mechanical properties of the as-processed (T0) foams and typical compression true stress-strain curves are shown in Figure 5A. A critical value of stress (σ_c), defined as the first maximum stress value, could

be identified for all the samples, but more clearly for the 10% *Spirulina* foam. After the critical stress it was observed that the samples followed a brittle fracture as the compression test progressed, indicated by the curve pattern with peaks up and down until the sample collapses characteristic of this type of systems (Attenburrow, Goodband, Taylor, & Lillford, 1989). As deduced from Figure 5B, only the highest *Spirulina* loading resulted in a significant increase (95% confidence interval) in the critical stress (2966 ± 322 kPa for 10% *Spirulina*, as compared to 1505 ± 573 kPa, 1568 ± 310 kPa and 2011 ± 622 kPa for the pure starch, 1% *Spirulina* and 5% *Spirulina*, respectively). A similar trend of increased hardness has been previously reported with the addition of lower *Spirulina* contents into extruded starch (Barbara Franco Lucas, et al., 2017) and was attributed to the effect of proteins in restricting moisture accessibility towards starch. The slightly greater crystallinity of the samples containing *Spirulina* can also explain the hardness increase. On the other hand, the stiffness of the foams was not significantly affected, as suggested by their compression moduli (15000-25000 kPa) (cf. Figure 5C), which were within the range of previously reported values for extruded starch foams (Robin, et al., 2010). It should be noted that the larger standard deviation values for the pure starch foam reflect a greater structural heterogenity. As previously discussed, the microstructure of the extruded samples consisted of a porous network which may be described as a solid foam (cf. Figure 2 and Figure 3). The micromechanics of foam deformation during compresion starts by cell walls bending elastically, and giving rise to the initial linear region in the stress-strain curves, followed by structural colapse when a critical value of stress is reached (Ashby & Medalist, 1983). Ashby and Gibson demostrated that the ratio of the bulk density to the density of the cell wall material can be correlated to the critical stress and modulus of foams (Ashby, et al., 1983). The strongest sample (i.e. presenting the highest critical stress) would correspond to that with the greater bulk density and containing thinner cell walls and a higher number of cells

535 (10% *Spirulina*), whilst coarse structures with a lower number of cells would be the weakest
536 (pure starch and 1% *Spirulina*). The increased hardness of the 10% *Spirulina* foam is
537 expected to have some implications on the consumers' acceptance. This will be further
538 evaluated by sensory analyses in the future.
539

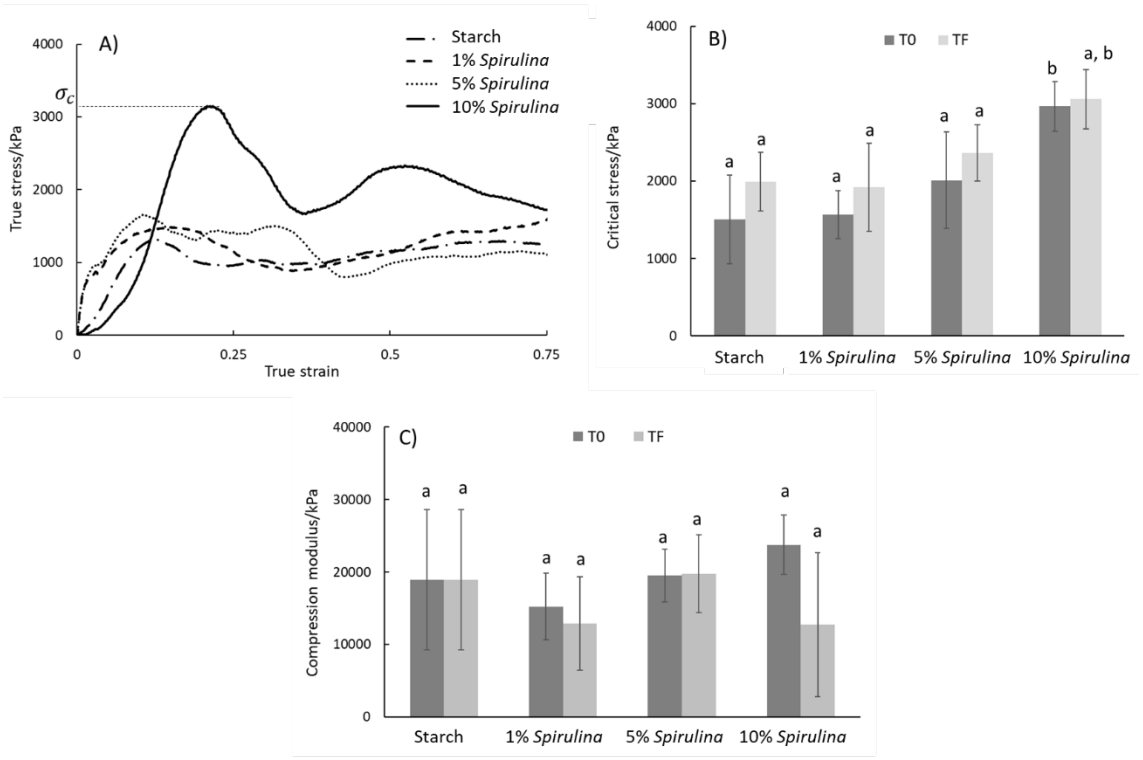

540

541 **Figure 5.** (A) Representative true stress vs strain curves of starch-*Spirulina* foams
542 conditioned at 30% RH. (B) Average critical stress for samples before (T0) and after storage
543 (TF). (C) Average compression modulus of the extruded samples before (T0) and after
544 storage (TF). Different letters indicate statistically significant differences between samples
545 ($p \leq 0.05$).
546

547 **3.2 Effect of retrogradation upon prolonged storage**

548 After being gelatinized, starch is capable of re-crystallizing upon storage at certain
549 conditions. During this re-crystallization process, known as retrogradation, the amylose

550 chains gradually re-associate and re-organize to form a different ordered structure (Wang,
551 Li, Copeland, Niu, & Wang, 2015). The impact of the *Spirulina* microalga on the
552 retrogradation process was evaluated by characterizing the obtained foams after storage at
553 30% RH for one month (TF). This would be representative of the properties of the foams
554 during their shelf-life. The nanostructural changes undergone by the samples at TF were
555 investigated by means of WAXS and SAXS. The WAXS patterns from the stored foams are
556 shown in Figure 6A. As observed, the crystalline structure of the foams changed from the
557 non-stable V-type mixture observed shortly after processing the samples (T0) towards a V_A
558 type structure, in agreement with what has been previously reported for other extruded starch
559 samples (Benito-González, et al., 2019; J. J. Van Soest, Hulleman, De Wit, & Vliegenthart,
560 1996). Additionally, two peaks located at ca. 17º and 22º, which are characteristic from the
561 B-type allomorph, were detected, suggesting that a certain fraction of starch re-crystallized
562 into this type of structure. Corn starch has been reported to re-crystallize into a B-type
563 structure when stored at low temperature (Shamai et al. 2003) or high relative humidity
564 conditions (Fu et al. 2013) and similar results have also been reported for corn starch samples
565 processed by means of melt compounding in the presence of 50 wt.% moisture (Benito-
566 González, et al., 2019). The re-crystallization into B-type structures has been related to the
567 rearrangement and association of the outermost short branches of amylopectin (Hoover,
568 Hughes, Chung, & Liu, 2010). The crystallinity values calculated for the foams at TF (cf.
569 Table 3) were very far from the value corresponding to the native starch (cf. Table 1) and
570 indicate that only a small fraction of starch was able to re-crystallize upon storage at
571 30% RH. The pure extruded starch and the hybrid foams presented very similar
572 crystallinities at TF and only the highest *Spirulina* loading gave rise to a slight crystallinity
573 increase compared to the pure starch. Comparing with the values estimated just after
574 processing (T0), the retrogradation process gave rise to a crystallinity increase of 92% in the

575 case of pure starch and 23% for the 1% *Spirulina* foam, whereas the crystallinity
576 corresponding to the starch fraction was slightly decreased for the 5% and 10% *Spirulina*
577 foams. It is known that greater moisture contents favour starch re-crystallization (J. Van
578 Soest & Knooren, 1997; Wang, et al., 2015) and in particular, the presence of moisture is
579 necessary for the transition of V-type complexes into B-type crystallites ((Kugimiya, et al.,
580 1980; Zobel, 1988). Previous studies have pointed out that the proteins present in *Spirulina*
581 may compete for water binding sites, hindering the hydration of starch granules (Batista, et
582 al., 2012; Barbara Franco Lucas, et al., 2017; Tańska, et al., 2017). These results confirm the
583 fact that the presence of the microalga limited the accessibility of moisture towards the starch
584 molecules and as a result, hindered the re-crystallization process. A similar effect has been
585 attributed to the presence of cellulose (Benito-González, et al., 2019) and other fillers which
586 interact with the hydroxyl groups from starch by the formation of hydrogen bonds (Ferrero,
587 Martino, & Zaritzky, 1994; Ghanbarzadeh, Almasi, & Entezami, 2011). It should be noted
588 that the 5% *Spirulina* and 10% *Spirulina* foams displayed additional weak peaks which
589 corresponded to the most intense scattering peaks from the raw *Spirulina*. This indicates that
590 the free fatty acids contained in the microalga were able to re-crystallize back to their native
591 form upon storage of the foams.
592
593 To confirm the effect of *Spirulina* on the crystallinity of the foams after storage, FT-IR
594 analyses were also carried out and the obtained spectra are shown in Figure S7. The spectral
595 region of 800–1200 cm^{-1} was used to investigate structural differences between samples, as
596 previous studies have suggested that bands in this 'fingerprint' region reflect changes in
597 polymer conformation and hydration of processed starches (Capron, Robert, Colonna,
598 Brogly, & Planchot, 2007; Htoon, et al., 2009; Sevenou, Hill, Farhat, & Mitchell, 2002; J. J.
599 G. van Soest & Vliegenthart, 1997). The band at 1022 cm^{-1} has been seen to increase in

600 more amorphous samples, while the bands at 1000 and 1047 cm^{-1} become more defined in
601 more crystalline samples (Capron, et al., 2007; Sevenou, et al., 2002; J. J. G. van Soest, et
602 al., 1997). In particular, the trend in the intensity ratio for the 1022:1000 bands has been
603 reported to correlate reasonably with the crystallinity measured by X-ray diffraction
604 (Capron, et al., 2007). The values here obtained for the 1022:1000 intensity ratio were
605 approximately constant (ca. 0.96-0.94) for all the samples, confirming that starch presented
606 a similar degree of crystallinity in all the foams after storage for one month.
607
608 Very broad and weak shoulders were detected in the SAXS patterns from the foams after
609 storage (cf. Figure 6B). This type of scattering feature has been previously detected for
610 retrogaded starches and has been assigned to the formation of heterogeneous semi-crystalline
611 structures (Shamai, Shimoni, & Bianco-Peled, 2004; Suzuki, Chiba, & Yarno, 1997). The
612 associated lamellar repeat distances ranged from ca. 51 nm for the pure starch to ca. 40-44
613 nm for the hybrid foams. Suzuki et al. reported lamellar distances of ca. 15-30 nm for potato
614 starch retrograded at low temperature (Suzuki, et al., 1997), whereas Shamai et al. noted the
615 appearance of a broad lamellar peak, characteristic of distances of ca. 20 nm, in high amylose
616 corn starch only when the samples were retrograded at low temperatures (Shamai, et al.,
617 2004). The broader shoulders observed for the hybrid foams indicate that the presence of
618 *Spirulina* promoted the re-crystallization of starch into more heterogeneous structures.
619 Furthermore, the power-law exponents in the low q region were 2.6-2.7 for all the samples,
620 confirming the existence of structures with low degree of order in the nanometre size range.
621 The slight increase in the power-law exponents of the foams at TF with respect to the
622 corresponding values at T0 confirm that the gelatinization process was irreversible and that
623 the neither the crystalline nor the lamellar structure of native starch were recovered upon
624 retrogradation. Presence of *Spirulina* and the effect of limited moisture accessibility

hindered the re-organization of amylose chains into crystalline domains and lamellae. However, all the foams presented very similar crystallinity values after storage since the mentioned effect upon storage was counteracted by the initially greater crystallinity of the hybrid foams at T0.

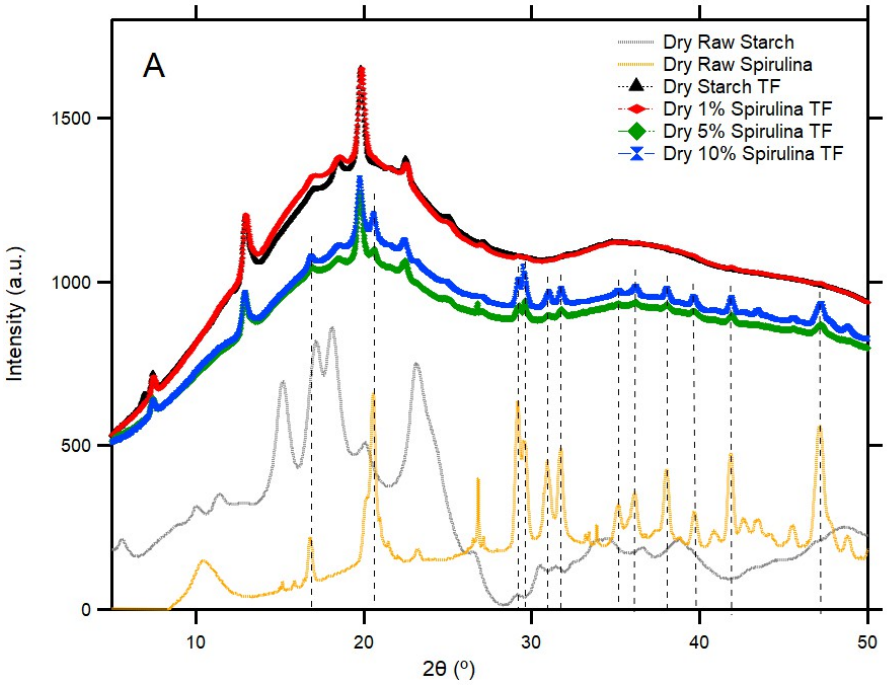

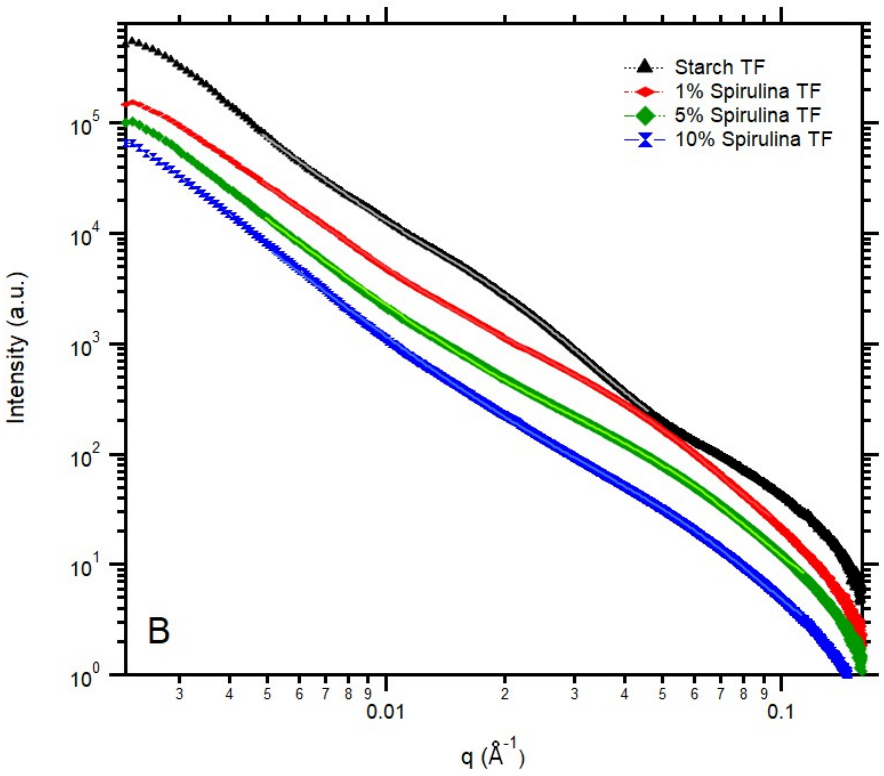

631

632 **Figure 6.** (A) WAXS patterns from the raw starch and *Spirulina* and from the foams after
633 storage for one month (TF) at 30% RH. Curves form raw starch and *Spirulina* have been
634 offset for clarity. (B) SAXS patterns from the fully hydrated samples. Dotted lines
635 correspond to the experimental data, whereas solid lines correspond to the fitting curves. The
636 curves have been offset for clarity.

637

638 **Table 3.** Power-law exponents, lamellar peak parameters and crystallinity (X_C) for the foams
639 after storage for one month (TF). The lamellar peak parameters were obtained by fitting the
640 experimental SAXS data of the hydrated samples to the sum function of a power-law plus a
641 Gaussian-Lorentzian peak and crystallinity was obtained from the peak fitting of the WAXS
642 patterns from the dry samples. Standard deviation values on the last digit are shown in
643 parentheses for the fitting parameters.

	Power-law exponent	Lamellar peak position ($Å^{-1}$)	Width of the lamellar peak ($Å^{-1}$)	Lamellar repeat distance (Å)	X_C (%)(*)
Starch	2.678 (9)	0.0122 (1)	0.0141 (1)	51.40	6.19 [6.19]
1% *Spirulina*	2.561 (7)	0.0156 (4)	0.0346 (1)	40.28	5.65 [5.65]
5% *Spirulina*	2.680 (2)	0.0144 (4)	0.0441 (1)	43.72	6.24 [5.90]
10% *Spirulina*	2.716 (4)	0.0143 (6)	0.0454 (1)	43.87	8.57 [7.75]

644 (*) The crystallinity values calculated accounting only for the contribution of starch are shown
645 in brackets.
646
647 As observed in Figure 5B, although the differences were not significant, partially due to a
648 large variability between replicates, a trend of increased hardness (i.e. greater critical stress
649 values) was observed when comparing the samples at T0 and TF, which could be expected
650 from the structural changes occurring during storage (i.e. the amorphous as-processed starch
651 foam may re-organize into more ordered structures upon storage, leading to the formation of
652 more mechanically resistant foams). The weak effect is reasonable considering the very
653 limited re-crystallization of starch after storage. The same trend observed at T0 was detected
654 for the foams after storage, i.e. the presence of higher amounts of *Spirulina* led to the
655 formation of harder foams, although the high standard deviation values for the measured
656 samples preclude from extracting definitive conclusions. Regarding stiffness, no significant
657 differences were observed between samples before and after storage, partly due to the large
658 variability between samples.
659
660 Since the crystalline structure of starch is known to have a significant impact on its
661 digestibility, the content of resistant starch (RS) was determined in the foams at TF,
662 obtaining values of 1.1 ± 0.3 g RS/100 g sample in the pure starch and the samples with 1%

and 5% *Spirulina* and a higher content of 2.1 ± 0.7 g RS/100 g sample in the foam with 10% *Spirulina*. This effect might be related to the formation of V-type amylose-lipid complexes, which has been previously noted in starch-*Spirulina* blends (Martínez-Sanz, et al., 2018) and as suggested by the WAXS patterns of the as-processed foams. These complexes are known to form more stable crystalline structures than those found in native starches. For instance, the formation of V-type amylose-lipid complexes has been shown to produce a decrease in the amylose solubility, hence increasing the gelatinisation temperature (Eliasson, Carlson, & Larsson, 1981). Furthermore, although amylose-lipid complexes are hydrolysed and absorbed in the gastrointestinal tract to the same extent as free amylose, the hydrolysis process has been seen to take place at a slower rate (J. Holm, et al., 1983). From a food design point of view, a higher content of resistant starch is desirable, since it is related to lower calorie content and lower glycaemic loads (Fuentes-Zaragoza, Riquelme-Navarrete, Sánchez-Zapata, & Pérez-Álvarez, 2010). Thus, the addition of 10% *Spirulina* could be interesting from a nutritional perspective, not only due to the increased protein content and the antioxidant properties provided by bioactive compounds such as polyphenols (De Marco, et al., 2014), but also due to the potential benefits associated to an increased content of resistant starch in the foams.

4. Conclusions

Starch foams with different loadings (1, 5 and 10 wt.%) of the microalga *Spirulina* were produced by means of extrusion cooking. The gelatinization process taking place during the extrusion process led to the disruption of the crystalline and lamellar structure of native starch, producing very amorphous foams. Furthermore, the crystallized fatty acids present in the raw *Spirulina* were completely melted. The release of *Spirulina* intracellular

components promoted the formation of more stable V-type complexes with amylose, leaving slightly more crystalline foams after processing. The microstructure of the foams was strongly affected by the presence of the microalga and the hybrid foams exhibited more densely packed and well-connected porous structures. This, in turn, affected the textural properties of the foams, which became harder with higher *Spirulina* loadings.

All the foams presented a very limited re-crystallization upon storage, being this further reduced in the case of the hybrid foams. As a result, all the foams presented similar crystallinity values after storage. Furthermore, the starch lamellar arrangement was only partially recovered, forming much more heterogeneous structures than those found in the native starch. The formation of amylose complexes was translated into a higher resistant starch content in the 10% *Spirulina* foam. This, together with the increased protein content and the presence of bioactive compounds such as polyphenols, highlights the potential benefits of adding *Spirulina* into starch extruded foams to produce snack foods with higher nutritional value.

These results show that the combination of advanced characterization tools such as X-ray scattering techniques and neutron tomography can provide very valuable information on the nano- and microstructure of starch-based products, which will ultimately enable a rational design of food products with the desired characteristics according to the consumers' requirements.

Acknowledgements

Synchrotron experiments were performed at NCD beamline at ALBA Synchrotron with the collaboration of ALBA staff (2016021658 project). Part of this work was supported by the

COST Action ES1408 European network for algal-bioproducts (EUALGAE). Roland Kádár, Chalmers University of Technology, Sweden, is gratefully acknowledged for access to the extruder. We acknowledge, LLB, Saclay, France for offering beamtime at the IMAGINE beamline. Ana Miljkovic is acknowledged for resistant starch and compression test measurements.

References

ALBA synchrotron. https://www.cells.es/en.

Anton, A. A., Gary Fulcher, R., & Arntfield, S. D. (2009). Physical and nutritional impact of fortification of corn starch-based extruded snacks with common bean (Phaseolus vulgaris L.) flour: Effects of bean addition and extrusion cooking. *Food Chemistry, 113*(4), 989-996.

Ashby, M. F., & Medalist, R. M. (1983). The mechanical properties of cellular solids. *Metallurgical Transactions A, 14*(9), 1755-1769.

Attenburrow, G., Goodband, R., Taylor, L., & Lillford, P. (1989). Structure, mechanics and texture of a food sponge. *Journal of Cereal Science, 9*(1), 61-IN61.

Batista, A. P., Nunes, M. C., Fradinho, P., Gouveia, L., Sousa, I., Raymundo, A., & Franco, J. M. (2012). Novel foods with microalgal ingredients–Effect of gel setting conditions on the linear viscoelasticity of Spirulina and Haematococcus gels. *Journal of Food Engineering, 110*(2), 182-189.

Bear, J. (2013). *Dynamics of fluids in porous media*: Courier Corporation.

Benito-González, I., López-Rubio, A., & Martínez-Sanz, M. (2019). High-performance starch biocomposites with celullose from waste biomass: Film properties and retrogradation behaviour. *Carbohydrate Polymers, 216*, 180-188.

Benito-González, I., Martínez-Sanz, M., & Lopez-Rubio, A. (2018). Potential of lignocellulosic fractions from *Posidonia oceanica* to improve barrier and mechanical properties of bio-based packaging materials. *International Journal of Biological Macromolecules, 118*, 542-551.

Blazek, J., & Gilbert, E. P. (2011). Application of small-angle X-ray and neutron scattering techniques to the characterisation of starch structure: A review. *Carbohydrate Polymers, 85*(2), 281-293.

Boussiba, S., & Richmond, A. E. (1979). Isolation and characterization of phycocyanins from the blue-green alga Spirulina platensis. *Archives of Microbiology, 120*(2), 155-159.

Bressani, R., Wilson, D. L., Béhar, M., & Scrimshaw, N. S. (1960). Supplementation of cereal proteins with amino acids: III. Effect of amino acid supplementation of wheat flour as measured by nitrogen retention of young children. *The Journal of nutrition, 70*(2), 176-186.

Brun, F., Mancini, L., Kasae, P., Favretto, S., Dreossi, D., & Tromba, G. (2010). Pore3D: A software library for quantitative analysis of porous media. *Nuclear Instruments and Methods in Physics Research Section A: Accelerators, Spectrometers, Detectors and Associated Equipment, 615*(3), 326-332.

754 Brun, F., Massimi, L., Fratini, M., Dreossi, D., Billé, F., Accardo, A., Pugliese, R., &
755 Cedola, A. (2017). SYRMEP Tomo Project: a graphical user interface for
756 customizing CT reconstruction workflows. *Advanced structural and chemical*
757 *imaging, 3*(1), 4.
758 Camire, M. E., Camire, A., & Krumhar, K. (1990). Chemical and nutritional changes in
759 foods during extrusion. *Critical Reviews in Food Science and Nutrition, 29*(1),
760 35-57.
761 Capron, I., Robert, P., Colonna, P., Brogly, M., & Planchot, V. (2007). Starch in
762 rubbery and glassy states by FTIR spectroscopy. *Carbohydrate Polymers, 68*(2),
763 249-259.
764 Chacón-Lee, T., & González-Mariño, G. E. (2010). Microalgae for "healthy" foods—
765 possibilities and challenges. *Comprehensive Reviews in Food Science and Food*
766 *Safety, 9*(6), 655-675.
767 Chanvrier, H., Uthayakumaran, S., Appelqvist, I. A. M., Gidley, M. J., Gilbert, E. P., &
768 López-Rubio, A. (2007). Influence of Storage Conditions on the Structure,
769 Thermal Behavior, and Formation of Enzyme-Resistant Starch in Extruded
770 Starches. *Journal of Agricultural and Food Chemistry, 55*(24), 9883-9890.
771 De Marco, E. R., Steffolani, M. E., Martínez, C. S., & León, A. E. (2014). Effects of
772 spirulina biomass on the technological and nutritional quality of bread wheat
773 pasta. *LWT-Food Science and Technology, 58*(1), 102-108.
774 Ding, Q.-B., Ainsworth, P., Plunkett, A., Tucker, G., & Marson, H. (2006). The effect
775 of extrusion conditions on the functional and physical properties of wheat-based
776 expanded snacks. *Journal of Food Engineering, 73*(2), 142-148.
777 Ding, Q.-B., Ainsworth, P., Tucker, G., & Marson, H. (2005). The effect of extrusion
778 conditions on the physicochemical properties and sensory characteristics of rice-
779 based expanded snacks. *Journal of Food Engineering, 66*(3), 283-289.
780 Fabra, M. J., Martínez-Sanz, M., Gomez-Mascaraque, L. G., Coll, J. M., Martínez, J. C.,
781 & Lopez-Rubio, A. (2017). Development and characterization of hybrid corn
782 starch-microalgae films: effect of US pre-treatment on structural, barrier and
783 mechanical performance. *Carbohydrate Polymers, under review*.
784 Ferrero, C., Martino, M., & Zaritzky, N. (1994). Corn starch-xanthan gum interaction
785 and its effect on the stability during storage of frozen gelatinized suspension.
786 *Starch-Stärke, 46*(8), 300-308.
787 Fradique, M., Batista, A. P., Nunes, M. C., Gouveia, L., Bandarra, N. M., & Raymundo,
788 A. (2010). Incorporation of Chlorella vulgaris and Spirulina maxima biomass in
789 pasta products. Part 1: Preparation and evaluation. *Journal of the Science of*
790 *Food and Agriculture, 90*(10), 1656-1664.
791 Fuentes-Zaragoza, E., Riquelme-Navarrete, M., Sánchez-Zapata, E., & Pérez-Álvarez,
792 J. (2010). Resistant starch as functional ingredient: A review. *Food Research*
793 *International, 43*(4), 931-942.
794 Furlan, K. P., Larsson, E., Diaz, A., Holler, M., Krekeler, T., Ritter, M., Petrov, A. Y.,
795 Eich, M., Blick, R., & Schneider, G. A. (2018). Dataset of ptychographic X-ray
796 computed tomography of inverse opal photonic crystals produced by atomic
797 layer deposition. *Data in brief, 21*, 1924-1936.
798 Ghanbarzadeh, B., Almasi, H., & Entezami, A. A. (2011). Improving the barrier and
799 mechanical properties of corn starch-based edible films: Effect of citric acid and
800 carboxymethyl cellulose. *Industrial Crops and Products, 33*(1), 229-235.
801 Guy, R. (2001). *Extrusion cooking: technologies and applications*: Woodhead
802 publishing.

Hashimoto, J. M., & Grossmann, M. V. E. (2003). Effects of extrusion conditions on quality of cassava bran/cassava starch extrudates. *International journal of food science & technology, 38*(5), 511-517.
Hildebrand, T., & Rüegsegger, P. (1997). A new method for the model-independent assessment of thickness in three-dimensional images. *Journal of Microscopy, 185*(1), 67-75.
Hoover, R., Hughes, T., Chung, H. J., & Liu, Q. (2010). Composition, molecular structure, properties, and modification of pulse starches: A review. *Food Research International, 43*(2), 399-413.
Howe, E., Jansen, G., & Gilfillan, E. (1965). Amino acid supplementation of cereal grains as related to the world food supply. *The American journal of clinical nutrition, 16*(3), 315-320.
Htoon, A., Shrestha, A. K., Flanagan, B. M., Lopez-Rubio, A., Bird, A. R., Gilbert, E. P., & Gidley, M. J. (2009). Effects of processing high amylose maize starches under controlled conditions on structural organisation and amylase digestibility. *Carbohydrate Polymers, 75*(2), 236-245.
Jenkins, P., Comerson, R., Donald, A., Bras, W., Derbyshire, G., Mant, G., & Ryan, A. (1994). In situ simultaneous small and wide angle X-ray scattering: A new technique to study starch gelatinization. *Journal of Polymer Science Part B: Polymer Physics, 32*(8), 1579-1583.
Jenkins, P. J., Cameron, R. E., & Donald, A. M. (1993). A universal feature in the structure of starch granules from different botanical sources. *Starch-Stärke, 45*(12), 417-420.
Joshi, S. M., Bera, M., & Panesar, P. (2014). Extrusion cooking of maize/spirulina mixture: factors affecting expanded product characteristics and sensory quality. *Journal of Food Processing and Preservation, 38*(2), 655-664.
Karlsson, K., Larsson, E., Lorén, N., Stading, M., & Rigdahl, M. (2019). Extrusion Parameters for Foaming of a β-Glucan Concentrate. *Journal of Polymers and the Environment, 27*(6), 1167-1177.
Khan, Z., Bhadouria, P., & Bisen, P. S. (2005). Nutritional and Therapeutic Potential of Spirulina. *Current Pharmaceutical Biotechnology, 6*(5), 373-379.
Kuang, Q., Xu, J., Liang, Y., Xie, F., Tian, F., Zhou, S., & Liu, X. (2017). Lamellar structure change of waxy corn starch during gelatinization by time-resolved synchrotron SAXS. *Food Hydrocolloids, 62*, 43-48.
Kugimiya, M., Donovan, J., & Wong, R. (1980). Phase transitions of amylose-lipid complexes in starches: A calorimetric study. *Starch-Stärke, 32*(8), 265-270.
Launay, B., & Lisch, J. M. (1983). Twin-screw extrusion cooking of starches: Flow behaviour of starch pastes, expansion and mechanical properties of extrudates. *Journal of Food Engineering, 2*(4), 259-280.
Lazou, A., & Krokida, M. (2010). Structural and textural characterization of corn–lentil extruded snacks. *Journal of Food Engineering, 100*(3), 392-408.
Legland, D., Arganda-Carreras, I., & Andrey, P. (2016). MorphoLibJ: integrated library and plugins for mathematical morphology with ImageJ. *Bioinformatics, 32*(22), 3532-3534.
Limaye, A. (2012). Drishti: a volume exploration and presentation tool. In *Developments in X-ray Tomography VIII* (Vol. 8506, pp. 85060X): International Society for Optics and Photonics.

Lopez-Rubio, A., Htoon, A., & Gilbert, E. P. (2007). Influence of extrusion and digestion on the nanostructure of high-amylose maize starch. *Biomacromolecules, 8*(5), 1564-1572.

Lucas, B. F., de Morais, M. G., Santos, T. D., & Costa, J. A. V. (2018). Spirulina for snack enrichment: Nutritional, physical and sensory evaluations. *LWT, 90*, 270-276.

Lucas, B. F., Morais, M. G. d., Santos, T. D., & Costa, J. A. V. (2017). Effect of Spirulina addition on the physicochemical and structural properties of extruded snacks. *Food Science and Technology, 37*(SPE), 16-23.

Martínez-Sanz, M., Fabra, M. J., G. Gómez-Mascaraque, L., & López-Rubio, A. (2018). Structural effects of microalgae additives on the starch gelatinisation process. *Food Hydrocolloids, 77*, 257-269.

Martínez-Sanz, M., Gómez-Mascaraque, L. G., Ballester, A. R., Martínez-Abad, A., Brodkorb, A., & López-Rubio, A. (2019). Production of unpurified agar-based extracts from red seaweed Gelidium sesquipedale by means of simplified extraction protocols. *Algal Research, 38*, 101420.

Miranda, M. S., Cintra, R. G., Barros, S. B. M., & Mancini-Filho, J. (1998). Antioxidant activity of the microalga Spirulina maxima. *Brazilian Journal of Medical and Biological Research, 31*, 1075-1079.

Morsy, O., Sharoba, A. E.-D., & Hem, B. (2014). Production and evaluation of extruded food products by using spirulina algae. *Annals of Agric. Sci., Moshtohor ISSN*, 1110-0419.

Onwulata, C., Konstance, R., Smith, P., & Holsinger, V. (2001). Co-extrusion of dietary fiber and milk proteins in expanded corn products. *LWT-Food Science and Technology, 34*(7), 424-429.

Ott, F., Loupiac, C., Désert, S., Hélary, A., & Lavie, P. (2015). IMAGINE: A cold neutron imaging station at the Laboratoire Léon Brillouin. *Physics Procedia, 69*, 67-70.

Özyurt, G., Uslu, L., Yuvka, I., Gökdoğan, S., Atci, G., Ak, B., & Işik, O. (2015). Evaluation of the cooking quality characteristics of pasta enriched with Spirulina platensis. *Journal of Food Quality, 38*(4), 268-272.

Parfitt, A. M., Drezner, M. K., Glorieux, F. H., Kanis, J. A., Malluche, H., Meunier, P. J., Ott, S. M., & Recker, R. R. (1987). Bone histomorphometry: Standardization of nomenclature, symbols, and units: Report of the asbmr histomorphometry nomenclature committee. *Journal of Bone and Mineral Research, 2*(6), 595-610.

Pastor-Cavada, E., Drago, S. R., González, R. J., Juan, R., Pastor, J. E., Alaiz, M., & Vioque, J. (2011). Effects of the addition of wild legumes (Lathyrus annuus and Lathyrus clymenum) on the physical and nutritional properties of extruded products based on whole corn and brown rice. *Food Chemistry, 128*(4), 961-967.

Rampersad, R., Badrie, N., & Comissiong, E. (2003). Physico-chemical and Sensory Characteristics of Flavored Snacks from Extruded Cassava/Pigeonpea Flour. *Journal of Food Science, 68*(1), 363-367.

Robin, F., Engmann, J., Pineau, N., Chanvrier, H., Bovet, N., & Della Valle, G. (2010). Extrusion, structure and mechanical properties of complex starchy foams. *Journal of Food Engineering, 98*(1), 19-27.

Rueden, C. T., Schindelin, J., Hiner, M. C., DeZonia, B. E., Walter, A. E., Arena, E. T., & Eliceiri, K. W. (2017). ImageJ2: ImageJ for the next generation of scientific image data. *BMC bioinformatics, 18*(1), 529.

Santos, T. D., Freitas, B. C. B. d., Moreira, J. B., Zanfonato, K., & Costa, J. A. V. (2016). Development of powdered food with the addition of Spirulina for food supplementation of the elderly population. *Innovative Food Science & Emerging Technologies, 37*, 216-220.

Sevenou, O., Hill, S. E., Farhat, I. A., & Mitchell, J. R. (2002). Organisation of the external region of the starch granule as determined by infrared spectroscopy. *International Journal of Biological Macromolecules, 31*(1), 79-85.

Shamai, K., Shimoni, E., & Bianco-Peled, H. (2004). Small angle X-ray scattering of resistant starch type III. *Biomacromolecules, 5*(1), 219-223.

Singleton, V. L., Orthofer, R., & Lamuela-Raventós, R. M. (1999). [14] Analysis of total phenols and other oxidation substrates and antioxidants by means of folin-ciocalteu reagent. In *Methods in enzymology* (Vol. 299, pp. 152-178): Elsevier.

Sommer, C., Straehle, C., Koethe, U., & Hamprecht, F. A. (2011). Ilastik: Interactive learning and segmentation toolkit. In *2011 IEEE international symposium on biomedical imaging: From nano to macro* (pp. 230-233): IEEE.

Spolaore, P., Joannis-Cassan, C., Duran, E., & Isambert, A. (2006). Commercial applications of microalgae. *Journal of Bioscience and Bioengineering, 101*(2), 87-96.

Suzuki, T., Chiba, A., & Yarno, T. (1997). Interpretation of small angle x-ray scattering from starch on the basis of fractals. *Carbohydrate Polymers, 34*(4), 357-363.

Tańska, M., Konopka, I., & Ruszkowska, M. (2017). Sensory, physico-chemical and water sorption properties of corn extrudates enriched with spirulina. *Plant foods for human nutrition, 72*(3), 250-257.

Van Soest, J., & Knooren, N. (1997). Influence of glycerol and water content on the structure and properties of extruded starch plastic sheets during aging. *Journal of Applied Polymer Science, 64*(7), 1411-1422.

Van Soest, J. J., Hulleman, S., De Wit, D., & Vliegenthart, J. (1996). Crystallinity in starch bioplastics. *Industrial Crops and Products, 5*(1), 11-22.

van Soest, J. J. G., & Vliegenthart, J. F. G. (1997). Crystallinity in starch plastics: consequences for material properties. *Trends in biotechnology, 15*(6), 208-213.

Veronica, A. O., Olusola, O. O., & Adebowale, E. A. (2006). Qualities of extruded puffed snacks from maize/soybean mixture. *Journal of Food Process Engineering, 29*(2), 149-161.

Vigani, M., Parisi, C., Rodríguez-Cerezo, E., Barbosa, M. J., Sijtsma, L., Ploeg, M., & Enzing, C. (2015). Food and feed products from micro-algae: Market opportunities and challenges for the EU. *Trends in Food Science & Technology, 42*(1), 81-92.

Wang, S., Li, C., Copeland, L., Niu, Q., & Wang, S. (2015). Starch Retrogradation: A Comprehensive Review. *Comprehensive Reviews in Food Science and Food Safety, 14*(5), 568-585.

Zobel, H. (1988). Starch crystal transformations and their industrial importance. *Starch-Stärke, 40*(1), 1-7.

Supplementary Material

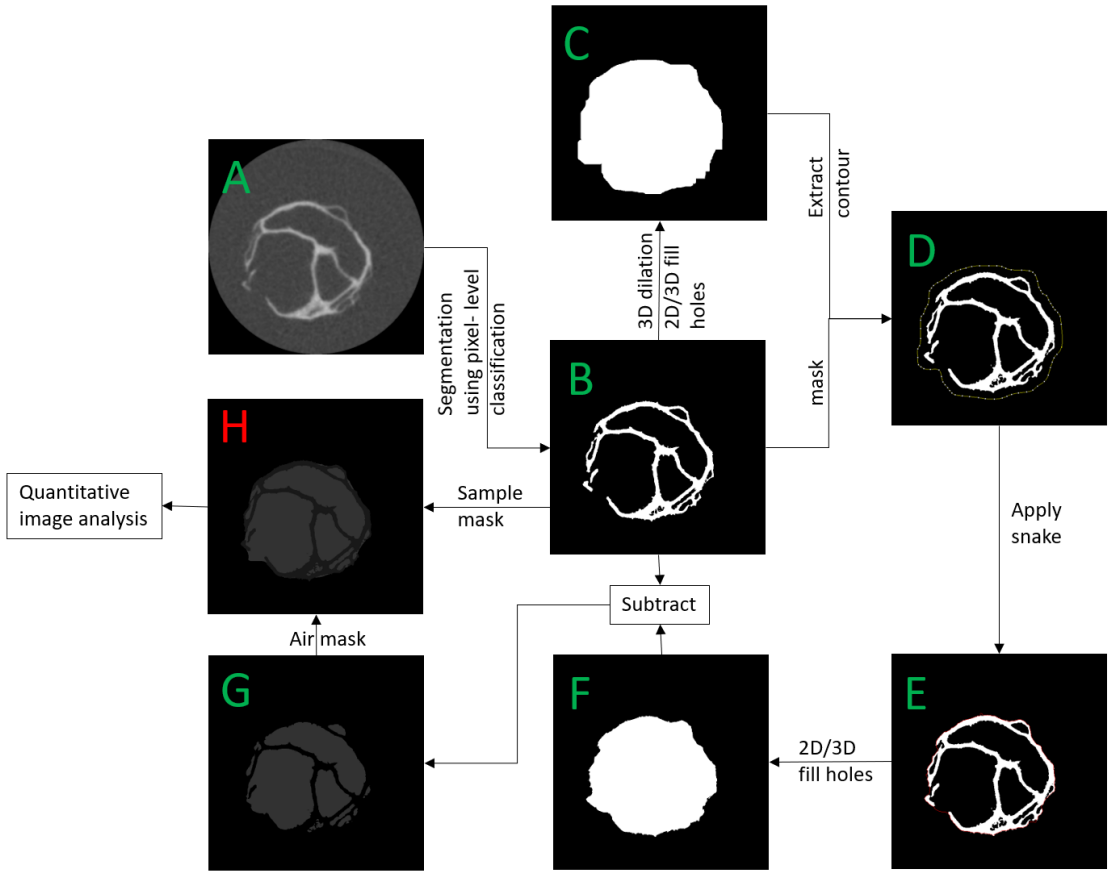

Figure S1. Schematic drawing of the applied 2D/3D image processing protocol in order to segment the extruded samples with broken cell walls experiencing an open-air macro pore connection, thus allowing further quantitative 3D image analysis. The original image (A) with a varying grey-scale value for the thinner and thicker cell wall, as well as with physically broken cell wall, is segmented using a pixel-level classification method implemented in 'Ilastik'. The resulting image (B) shows a pore connected to the outer air, via a thin broken cell wall, which impedes further 3D quantification of the air skeleton and quantification of both the connectivity density and pore size distribution. (C-G) shows the utilized image processing steps, finally resulting in image (H), where the extruded sample and the air pore space have been successfully segmented from the background. All image

processing steps were performed in 3D. The results of these steps were used for both quantitative image analysis and 3D-renderings.

Representative Volume of Interest (RVI) test

Quantitative 3D image analysis is commonly applied on so called volume of interests (VOIs), which are often cubic, and extracted from different positions inside the sample, far away from sample borders, which can often be non-representative to include in such an analysis. The size of the considered VOI is determined by a prior Representative Volume of Interest test (RVI-test) (Bear, 2013), where the quantified parameters, e.g. Volume percentage (Vol.Perc.) and Connectivity Density (Conn.D) are plotted against the side length of the VOI, as shown in Figures S2 and S3. The representative VOI-size is found when the observed parameters 'level out' and are no longer affected by the varying size of the considered VOI (Bear, 2013). Such an approach also works well on extruded samples with a rather low porosity and a thick cell wall structure of the extrudate, as shown in (Karlsson, Larsson, Lorén, Stading, & Rigdahl, 2019). However, for extruded samples with a very high porosity, large pore size and very thin cell wall structure, as for the hereby described extruded foams with a high starch content, quantitative analysis based on cubic VOIs is challenging, due to the fact that the quantified parameters fail to 'level out', even for the maximum possible applied VOI-size, following the RVI-test. Therefore, a modified RVI-test, where the sample diameter is kept 'as is' and only the height of the VOI is allowed to vary, was performed. For the given samples, a representative VOI height of 11.2 mm and 7.1 and was found for the pure starch and hybrid starch-*Spirulina* foams, respectively, as shown in Figures S2 and S3.

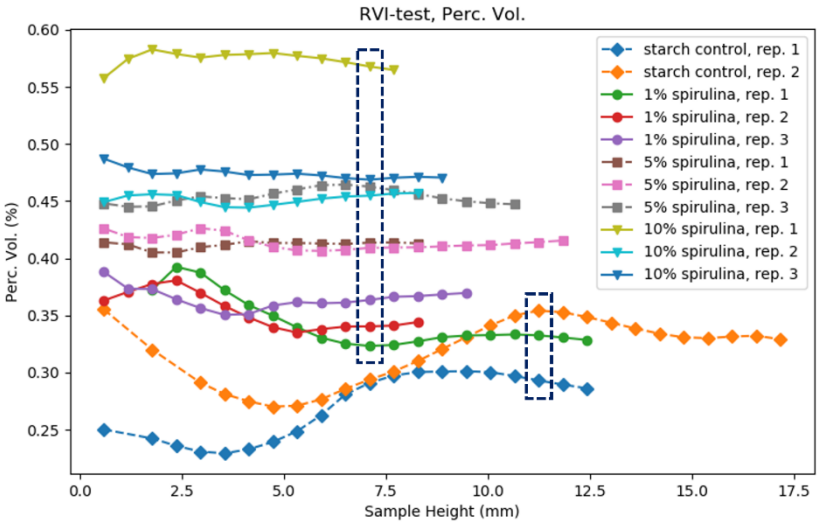

977

978 **Figure S2.** Test for finding the representative volume of interest (RVI-test), based on the
979 Vol. Perc. as the evaluation parameter. The optimal height of the VOI was chosen at 11.2
980 mm and 7.1 mm for the starch and hybrid starch-*Spirulina* foams, respectively.

981

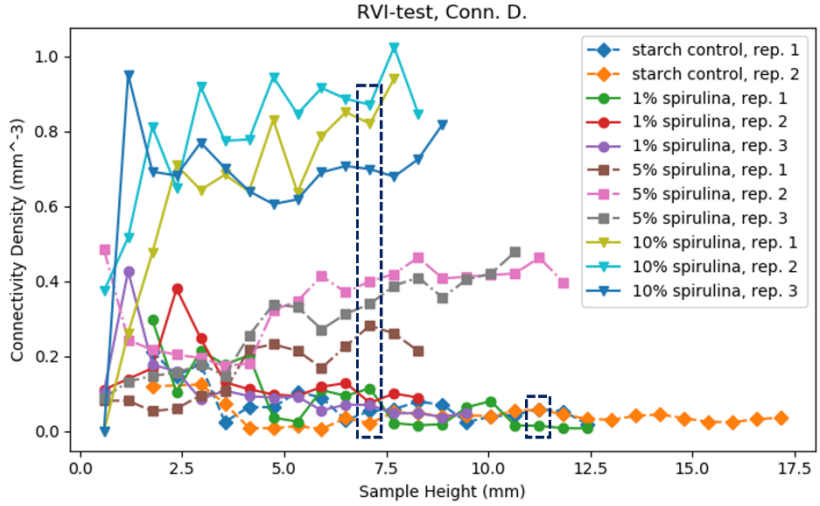

982

983 **Figure S3.** Test for finding the representative volume of interest (RVI-test), based on the
984 Conn. D. as the control parameter. The optimal height of the VOI was chosen at 11.2 mm
985 and 7.1 mm for the starch and hybrid starch-*Spirulina* foams, respectively.

986

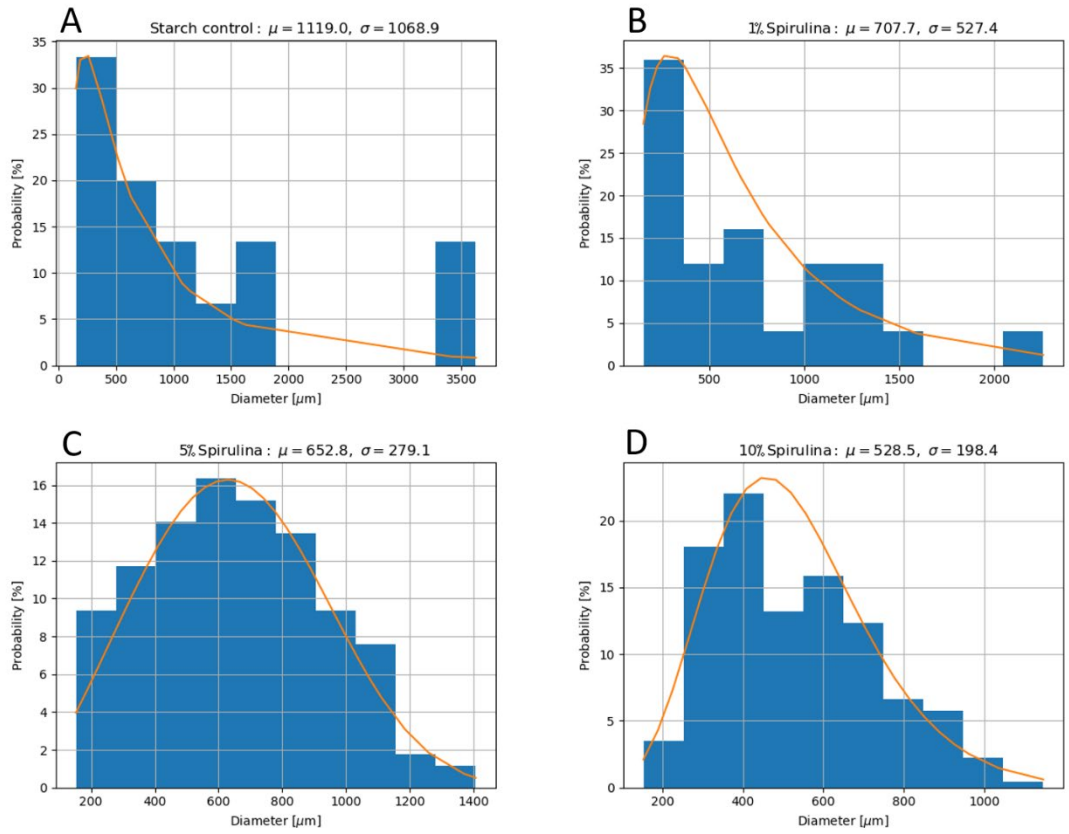

Figure S4. Pore size distribution of the extruded foams (A) pure starch, (B) 1% *Spirulina*, (C) 5% *Spirulina* and (D) 10% *Spirulina,* as quantified by Method 1. A Weibull distribution (orange) was used to fit the data. The fitting works rather accurately for continuous pore sizes up to 1400 μm as in (C-D) but fails at pore sizes bigger than 2000 μm as in (A-B), due to the discrete number of available pores.

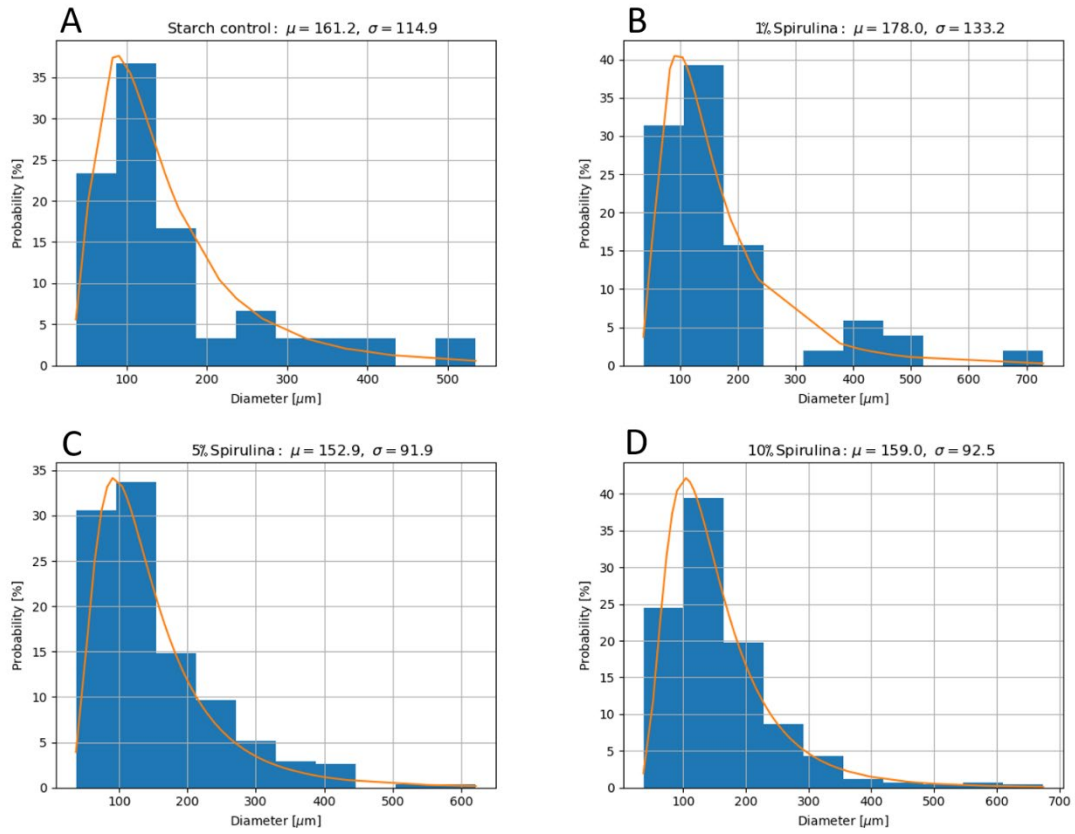

994

995 **Figure S5.** Throat size distribution of of the extruded foams (A) pure starch, (B) 1%
996 *Spirulina*, (C) 5% *Spirulina* and (D) 10% *Spirulina,* as quantified by Method 1. A Weibull
997 distribution (orange) was used to fit the data. The fitting works rather accurately for
998 continuous throat sizes in (C-D) and less well for the discrete throats sizes in (A-B)

999

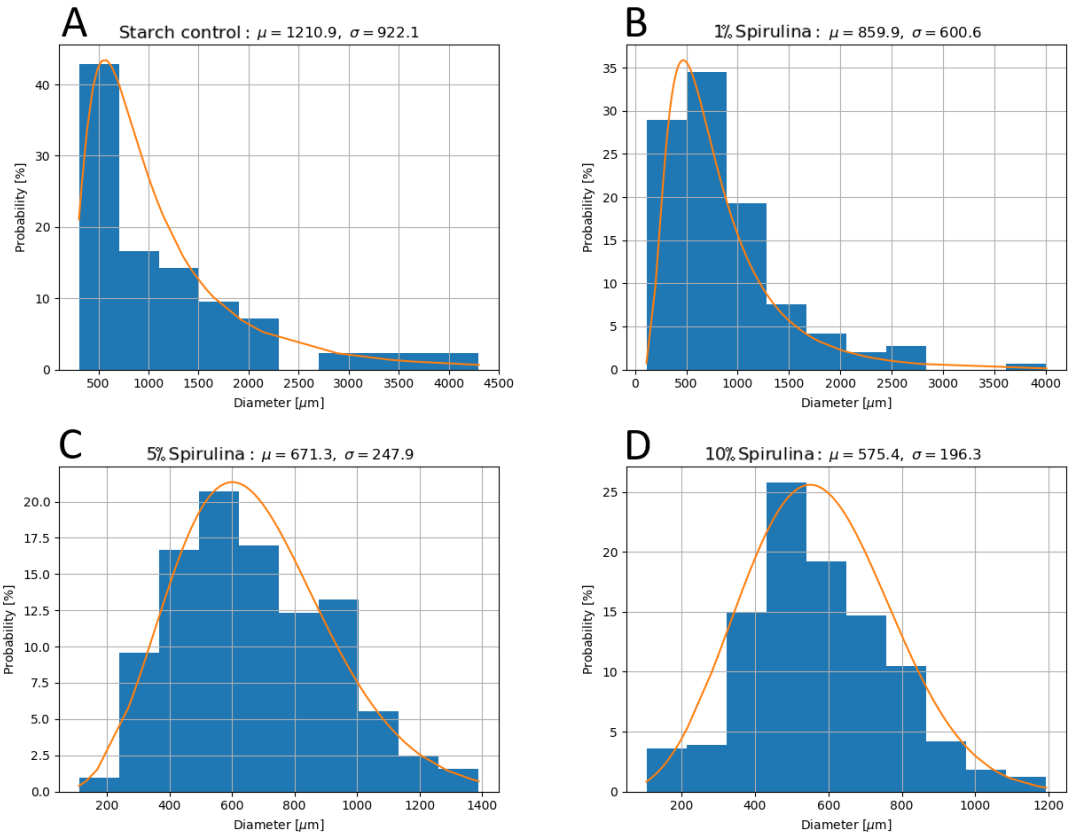

Figure S6. Pore size distribution of the extruded foams (A) pure starch, (B) 1% *Spirulina*, (C) 5% *Spirulina* and (D) 10% *Spirulina,* as quantified by Method 2. A Weibull distribution (orange) was used to fit the data. The fitting works rather accurately for all pore sizes (A-D).

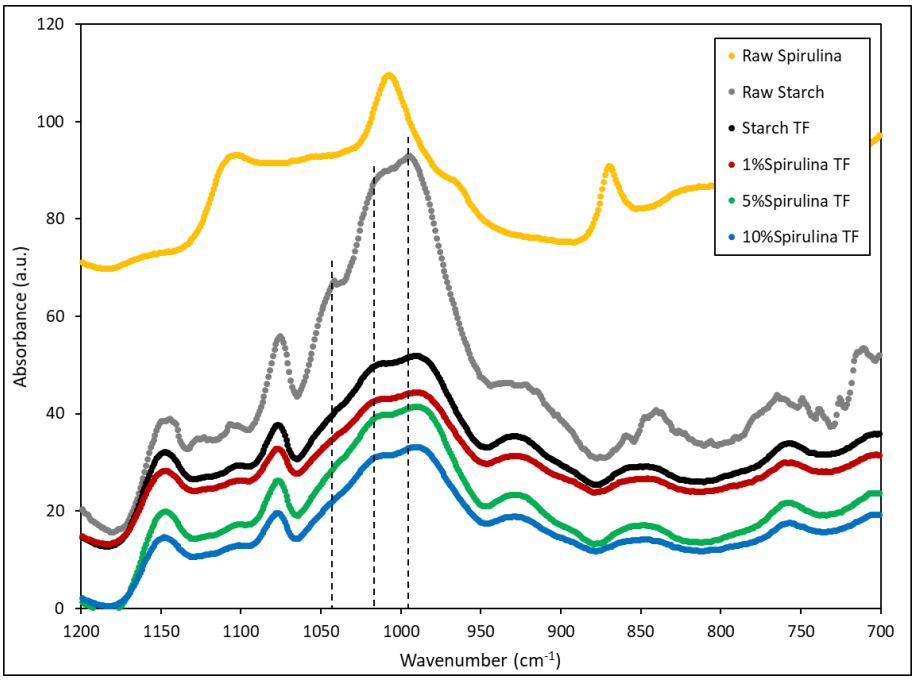

Figure S7. ATR-FTIR spectra from the raw starch and *Spirulina* and from the foams after storage. Curves have been offset for clarity.